High-K ankaramitic melt inclusions and lavas in the Upper Cretaceous Eastern Srednogorie continental arc, Bulgaria: Implications for the

Lithos 113 (2009) 228–245

Contents lists available at ScienceDirect

Lithos

journal homepage: www.elsevier.com/locate/lithos

High-K ankaramitic melt inclusions and lavas in the Upper Cretaceous Eastern Srednogorie continental arc, Bulgaria: Implications for the genesis of arc shoshonites

Peter Marchev [a,*], Svetoslav Georgiev [b], Zoltán Zajacz [b], Piero Manetti [c], Raya Raicheva [a], Albrecht von Quadt [b], Simone Tommasini [c]

[a] Geological Institute, Bulgarian Academy of Sciences, Acad. G. Bonchev Str., Bl. 24, 1113 Sofia, Bulgaria
[b] Isotope Geology and Mineral Resources, Department of Earth Sciences, ETH, Zürich, Sonneggstrasse 5, CH-8092, Zürich, Switzerland
[c] Dipartimento di Scienze della Terra, Università degli Studi di Firenze, via La Pira, 4, I-50121, Firenze, Italy

ARTICLE INFO

Article history:
Received 7 August 2008
Accepted 12 March 2009
Available online 24 March 2009

Keywords:
Ankaramites
Shoshonites
Melt inclusions
Olivine
Eastern Srednogorie

ABSTRACT

The Upper Cretaceous Yambol–Burgas region of the Eastern Srednogorie continental arc is characterized by unusually large volumes of mafic shoshonitic and ultra-K magmatism represented by high-Mg cumulitic rocks, and nepheline-normative ankaramites, absarokites and shoshonitic (high-alumina) basalts. The cumulitic rocks consist of phenocrysts of clinopyroxene and olivine (Fo_{91-85}) with inclusions of spinel (Cr#75–78). Olivine high-Fo cores and clinopyroxene host glassy melt inclusions which have nepheline-normative compositions with ankaramitic CaO/Al_2O_3 ratios (>1), low SiO_2 (47.4–50.0 wt.%), high MgO (7.5–10.8 wt.%), high total alkalis and shoshonitic K_2O/Na_2O ratios (>1). Electron microprobe and LA-ICPMS analyses demonstrate that parental magma was a high-Ca primitive mantle melt. Melt inclusions from the less Fo_{85} rim approach absarokite composition with CaO/Al_2O_3 ratios<1, lower MgO (5.2 wt.%), and higher total alkalis and K_2O/Na_2O ratio. The ankaramitic rocks are strongly porphyritic, composed of phenocrysts of altered olivine with spinel inclusions and large clinopyroxene. Their major and trace element compositions are similar to those of melt inclusions hosted in the high-Fo_{91-90} cores and clinopyroxene of the cumulitic rock. The absarokites differ from the high-K ankaramites by slightly higher SiO_2 (50.6–52.7 wt.%), Al_2O_3 and alkali-oxide contents, lower FeO and MgO and particularly low CaO/Al_2O_3 (0.6–0.9) ratio. Compared to the absarokites, shoshonitic basalts have similar SiO_2 (50.2–52.8 wt.%) at lower MgO contents and CaO/Al_2O_3 ratios (0.37–0.53). The presented extensive set of major and trace element data on melt inclusions and whole rocks, along with their main phenocryst compositions, is used to constrain the crystallization temperatures and pressures of the most primitive ankaramites. We suggest that ankaramite compositions are formed by melting of a garnet-free metasomatized mantle source rather than by melting of lower crustal cumulates. Numerical modelling demonstrates that the generation of absarokites and shoshonitic basalts is compatible with fractionation of olivine and clinopyroxene from ankaramitic magma. The high-Mg chemistry of cumulitic rocks is explained as the result of accumulation of these minerals.

1. Introduction

The identification of the most primitive magmas is a prime task in petrological studies of subduction-related magmatism. Primitive magma compositions are important because they nearly represent the composition of primary silicate melts and therefore can provide valuable information about the nature of the mantle source and the mantle melting processes. The most primitive rocks in many arcs with high-K (shoshonitic) volcanism are rare absarokites which are believed to represent the parental magmas (e.g. Hesse and Grove, 2003). In obvious contrast with the scarcity of mafic magmas in other island-arc environments (Lee and Stern, 1998; Hirschmann et al., 2000; Leat et al., 2002), the eastern segment of the Upper Cretaceous Srednogorie magmatic arc in Bulgaria is characterized by widespread mafic high-K (shoshonitic to ultrapotassic) rocks (Stanisheva, 1965, 1969, 1970; Stanisheva-Vassileva, 1980; Stanisheva-Vassileva and Daieva, 1990; Boccaletti et al., 1978; Manetti et al., 1979; Georgiev, 2008). In the Srednogorie magmatic arc, absarokites are accompanied by more primitive potassic ankaramites (high-Mg rocks with CaO/Al_2O_3 ratio ≥ 1; Marchev et al., 2007) and more evolved trachybasalts (shoshonitic high-Al basalts), shoshonites and latites. Similar rock associations are also typical for several other continental and oceanic shoshonitic series, e.g. the Aeolian Islands Volcanic Arc (Gioncada et al., 1998), the West Sulawesi Volcanic Province (Elburg et al., 2006) and Lihir Island, Papua New Guinea (Kennedy et al., 1990). This may signify that ankaramites, instead of absarokites, are the parental magma of the shoshonitic series.

The existence of ankaramitic magma, however, has been a subject of a long-standing debate. In the past, their high-Ca nature has been interpreted as the result of accumulation of clinopyroxene in normal

* Corresponding author.
E-mail address: pmarchev@geology.bas.bg (P. Marchev).

0024-4937/$ – see front matter © 2009 Elsevier B.V. All rights reserved.
doi:10.1016/j.lithos.2009.03.014

picrites or olivine basalts (Gunn et al., 1970; Hughes, 1982). Following the discovery of olivine-hosted melt inclusions with nepheline-normative ankaramitic compositions (Della-Pasqua and Varne, 1997; Gioncada et al., 1998), island-arc ankaramites have been designated as a distinctive magma type (Schiano et al., 2000). Recently, however, doubt has been also cast on the ankaramitic characteristics of the melt inclusions in the high-Mg olivines. For example, Gaetani et al. (2002) suggested that the high-CaO contents and CaO/Al_2O_3 ratios of melt inclusions in high-Mg olivine reflected diffusion of Ca through the olivine lattice, whereas Danyushevsky et al. (2004) concluded that they were the result of local melting reactions.

In this paper we address three major issues: (1) does the high-K ankaramitic magma exist and if it does, (2) is it the most primitive composition in the shoshonitic series; and (3) what is its genetic relationship with the more evolved lavas? To address these issues we present our study on the petrology and geochemistry of mafic Upper Cretaceous high-K (shoshonitic) rocks (ankaramites, absarokites and high-K high-Al basalts), along with data from ankaramitic melts trapped in the phenocrysts of an ultramafic cumulitic rock. Our data show a clear correlation between the compositions of the melt inclusions enclosed in olivine and clinopyroxene phenocrysts in this cumulitic rock and the bulk compositions of ankaramitic lavas, providing firm evidence for the existence of high-K ankaramitic melts. Our observations are consistent with other studies of arc-related ankaramites and with the hypothesis that they represent a distinct magma type. We also show that this particular magma type is the best candidate as the parental magma of the more differentiated shoshonitic and high-K magmas in the area.

2. Geological setting and sampling

2.1. Apuseni–Banat–Timok–Srednogorie Belt and Srednogorie zone

The Eastern Srednogorie zone is the easternmost segment of a >1000 km long and 30–70 km wide belt of Upper Cretaceous calc-alkaline and shoshonitic magmatic rocks in SE Europe that extends from the Apuseni Mts (Romania) in the NW, through the Timok zone (Serbia) and to the Srednogorie zone (Bulgaria) in the east (Jankovic, 1997; Popov et al., 2002) (Fig. 1). The Apuseni–Banat–Timok–Srednogorie (ABTS) belt represents a continental margin magmatic arc, whose tectonic evolution broadly relates to subduction processes prior to the Upper Cretaceous collision events (Ciobanu et al., 2002). Paleomagnetic studies show that the present sinusoidal L shape of the belt is a result of an ~80° clockwise rotation of the Apuseni Mountains and Banat sectors during the Tertiary (Patrascu et al., 1992, 1994; Csontos, 1995; Fügenschuh and Schmid, 2005).

Two different tectonic concepts for the origin of the ABTS belt have been proposed almost simultaneously in the early 1970s. Subduction of the Vardar ocean (branch of Tethian ocean) beneath the Serbo–Macedonian–Rhodope Massif has been suggested by Dewey et al. (1973) and Boccaletti et al. (1974) and later on accepted by most workers (e.g. Aiello et al., 1977; Hsu et al., 1977; Dabovski et al., 1991; Stampfli and Borel, 2004). In contrast, other tectonic interpretations consider the ABTS belt as an extensional structure that originated in an epicontinental rift environment that formed after the Early-Middle Cretaceous collisional deformations as a result of post-collisional

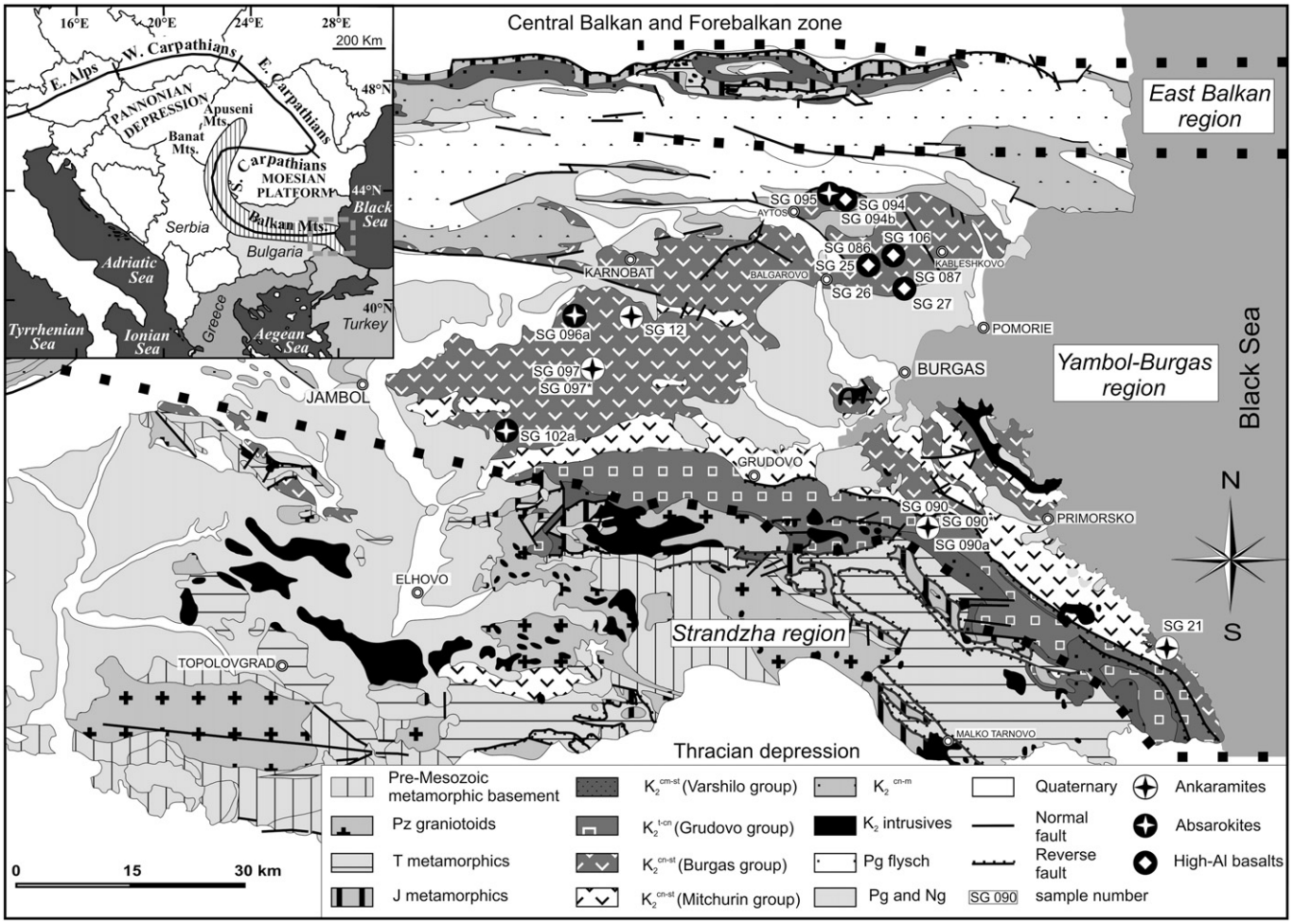

Fig. 1. Simplified geological map of the Eastern Srednogorie zone showing the location of the sampled primitive magmas (modified after Georgiev, 2008 based on Cheshitev and Kanchev, 1989). Inset shows entire Apuseni–Banat–Timok–Srednogorie Belt.

collapse and related asthenospheric diapirism (Antonijevic et al., 1974; Popov, 1981, 1987, Popov et al., 2002).

The Srednogorie zone is divided into 3 segments based on the major element geochemistry of the magmatic rocks, crustal thickness and geophysical characteristics: Western Srednogorie, Central Srednogorie and Eastern Srednogorie (Stanisheva-Vassileva, 1980; Dabovski et al., 1991). Unlike the Western and Central Srednogorie, which are characterized by predominantly basaltic–andesite, andesite and felsic calc-alkaline and shoshonitic magmatism, the Eastern Srednogorie segment consists of mafic volcanism with large variations of K_2O covering a range of island-arc series. Based on chemical variations of the igneous rocks, the Eastern Srednogorie zone is divided from south to north into 4 units: (1) Strandzha volcano-intrusive region; (2) Yambol–Burgas volcano-intrusive region; (3) North Burgas volcanic region and (4) Luda Kamchia (East Balkan) volcanic region (Dabovski et al., 1991). Our new data, however, show that there are no clear petrological differences between the Yambol–Burgas and the North Burgas regions. Therefore, we merge the latter unit into that of the Yambol–Burgas volcano-intrusive region.

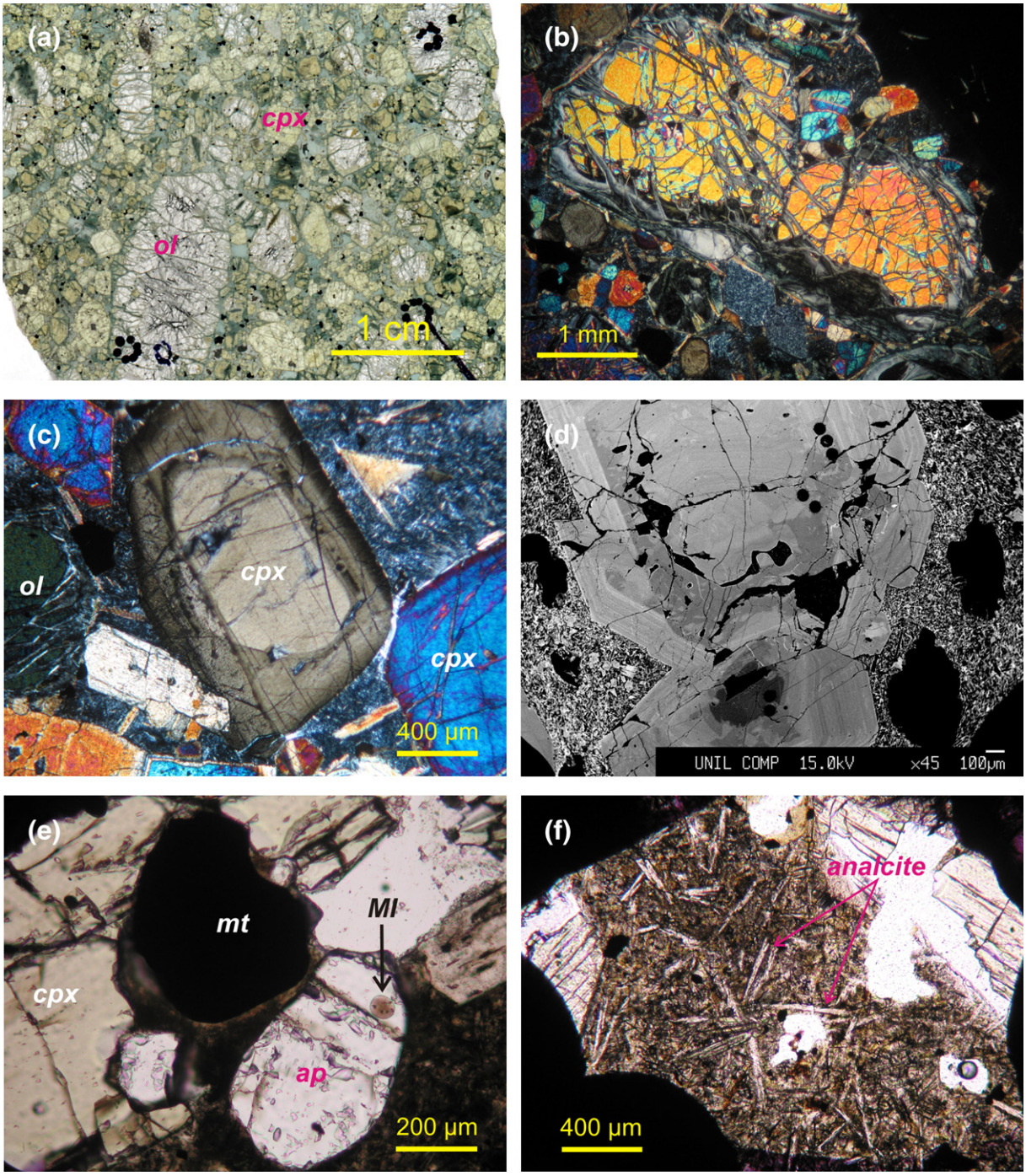

Fig. 2. (a) Photograph of polished thin-sections from the cumulate lava (SG12), demonstrating the size, morphology and abundance of the olivine (white) and clinopyroxene (light green) crystals. (b) Euhedral olivine crystal partly replaced by Mg–Fe hydrooxides. (c) Clinopyroxene crystal in SG12 with a rounded slightly zoned light gray core (Mg# 90.5–86) and outer zone (Mg# 82–69). (d) Backscattered-electron image of clinopyroxene crystals showing strongly corroded high-Mg black core (Mg# 91–88) surrounded by oscillatory outer zone Mg# 85–72 and very thin rim (Mg# 66). The core of the upper crystal seems to have been partly replaced by compositions similar to outer rims. (e) Large magnetite and apatite crystals from the shoshonitic basalts (SG106). Note the large melt inclusion (MI) in the apatite. (f) Large analcite microlites in the groundmass of the absarokite SG095. (For interpretation of the references to colour in this figure legend, the reader is referred to the web version of this article.)

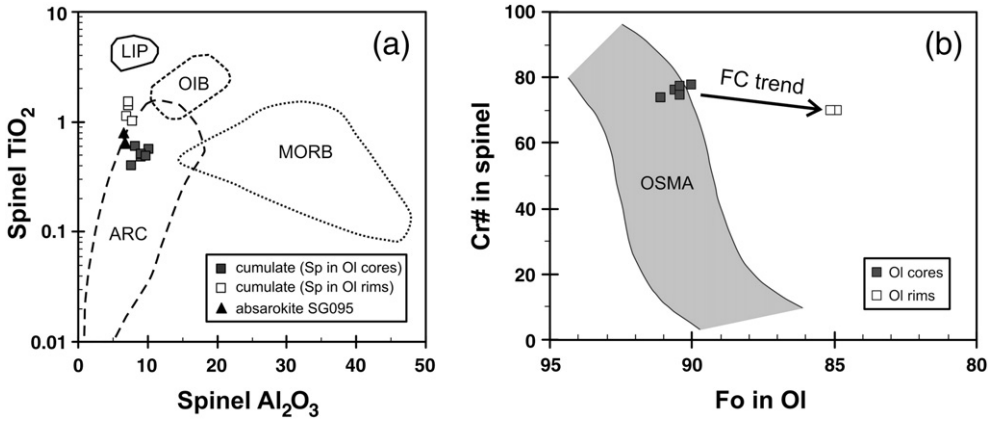

Fig. 3. (a) TiO_2 vs. Al_2O_3 for spinels from the Yambol–Burgas mafic rocks. Black line denotes magmatic spinel for MORB, OIB and ARC as described in Kamenetsky et al. (2001). (b) Spinel Cr# vs. host olivine Fo. The gray field in the diagram delineates the array of mantle spinels defined by Arai (1994). Fractional crystallization trend run from the mantle array towards lower Fo composition, as indicated by the arrow.

2.2. Yambol–Burgas volcano-intrusive region

Volcanic rocks from the Yambol–Burgas volcano-intrusive region form a thick pile of volcanic and volcano-sedimentary rocks. Drilling at site R-2 close to the town of Pomorie penetrated >3000 m of volcanic rocks without reaching the basement. The total thickness of the volcanic-derived sequence was estimated to exceed 6000 m in the eastern parts of the area (Stanisheva-Vassileva, 1989). Volcanic rocks, divided into 26 volcanic centers (Popov et al., 1993), were deposited in shallow to deep marine environments, forming predominantly pillow lavas and hyaloclastite breccias and rarely massive to columnar jointed lava flows. A large number of dykes occur in the region, particularly in the area of Aytos, which in some cases form E–W oriented dyke swarms. These dyke swarms probably represent important feeding structures (Ivanov, 1979).

Dabovski et al., in press have summarised the petrology and geochemistry of the Eastern Srednogorie, while the most comprehensive geochemical, isotopic and age dataset has recently been obtained by Georgiev (2008). Rocks from the Yambol–Burgas volcano-intrusive region chemically belong to the shoshonitic and ultrapotassic series, with most samples having mafic to intermediate composition and very rare felsic lithologies (Daieva and Stanisheva-Vassileva, 2002; Georgiev, 2008). The intermediate and felsic rocks are not considered further in this paper.

The primitive nature of the magmatism was first noted by Stanisheva (1965, 1968) and Boccaletti et al. (1978). These authors used a variety of terms to describe the Eastern Srednogorie mafic volcanic rocks, including picrites, limbourgite–augites, basanites, picro-basalts, absarokites and shoshonites (see also Daieva and Stanisheva-Vassileva, 2002). On the basis of rock composition and the deep-sea environment, the Yambol–Burgas volcano-intrusive area was interpreted as the rear and back-arc rift parts of the Srednogorie island-arc system (Georgiev et al., 2001). However, new U–Pb zircon age determinations (Georgiev, 2008) show that the igneous activity in the Yambol–Burgas region (81–78 Ma) is younger than that in the northern East Balkan region (~90 Ma); it is also younger, or partly overlapping with the magmatism in the southern Strandzha region (~86–78 Ma). These age data were interpreted by Georgiev (2008) in favour of an intra-arc rift rather than a back-arc system for the origin of Yambol–Burgas region. Such a model is consistent with geophysical data showing that the Yambol–Burgas region has the thinnest present-day crust in Bulgaria (~27 km; Yosifov and Pchelarov, 1977).

The location of the mafic rocks from this study is shown in Fig. 1. Brief information on the geographic location, composition and mode of occurrence is provided in Table 1 in the Appendix. For simplicity, throughout the paper we follow a petrographic division of the rocks into cumulates, ankaramites, absarokites and shoshonitic (high-Al) basalts. The ankaramites are most abundant in the Tamarino Bakadzhik paleovolcano, where numerous lava flows and sills, originally determined as picrites, have been described in drill holes, mining works and surface outcrops (Stanisheva, 1965). Other samples are lavas and dykes, taken from quarries and road-cuts throughout the area. The cumulitic rock from Dragantsi (SG12), which has fresh olivine containing ankaramitic melt inclusions, is a duplicate sample from the same ultramafic rock, previously described by Boccaletti et al. (1978) as picrite. It represents a small outcrop, strongly tectonically reworked. Because of the unclear relationship with the surrounding rocks, the morphology of the body is difficult to be determined, but most probably is either a small lava flow or a sill.

3. Analytical techniques

The major element composition of ankaramitic lavas and dykes were determined on fused pellets using a Phillips 2404 spectrometer at the University of Saltsburg, a WD-XRF, Axios, PANalytical spectrometer at the ETH Zurich, and a Philips PW2400 spectrometer at the University of Lausanne. Bulk rock major and trace element composition of the cumulitic sample were measured by XRF using a Philips PW1480 spectrometer at the University of Florence. MgO, Na_2O and FeO concentrations were determined by wet chemical analyses.

Major elements in minerals and glasses were analyzed by a JEOL 870 SUPERPROBE at the University of Florence and a JEOL SUPERP-

Table 1
Major and trace element composition of olivine in cumulate SG12 analyzed by LA-ICPMS.

	jn27a15	jn27a17	jn27b04	jn27b06	au28a03
SiO_2	40.83	41.05	40.42	40.43	41.12
TiO_2	0.00	0.01	0.00	0.00	<0.01
Al_2O_3	0.04	0.04	0.03	0.03	0.03
FeO	8.93	9.03	12.21	12.23	13.97
MnO	0.19	0.19	0.24	0.24	0.28
MgO	49.54	49.13	46.68	46.65	44.21
CaO	0.46	0.53	0.41	0.41	0.38
Na_2O	0.01	0.01	0.01	0.01	0.01
Total	100.00	100.00	100.00	100.00	100.00
Fo	90.8	90.6	87.2	87.2	84.9
P	23	52	27	27	204
Sc	5.06	2.99	6.03	6.02	5.77
V	1.26	2.53	1.00	1.00	<2.89
Cr	307	334	169	168	95
Ni	1102	1139	1048	1051	913
Cu	5.83	6.24	11.97	11.92	<16.51
Sr	0.16	0.34	0.08	0.08	<0.48
Y	0.05	<0.05	<0.05	<0.07	<0.58
Zr	0.01	<0.11	<0.15	<0.05	<0.40
B	<1.91	<1.93	6.03	<12.24	<30.21
Li	3.48	5.07	5.00	4.99	<9.25

ROBE JXA-8200 at ETH Zurich and the University of Lausanne. A 15 keV accelerating potential, 10 nA beam current and 1 μm beam diameter were used in Florence for minerals, whereas a defocused (5 μm diameter) probe was used for glass analyses. A 15 kV acceleration voltage, 15 nA beam current and 2 μm beam diameter was applied in Zurich and Lausanne. Natural and synthetic minerals were used as standards. Most reported analyses of minerals represent the average of at least 2 single-point analyses.

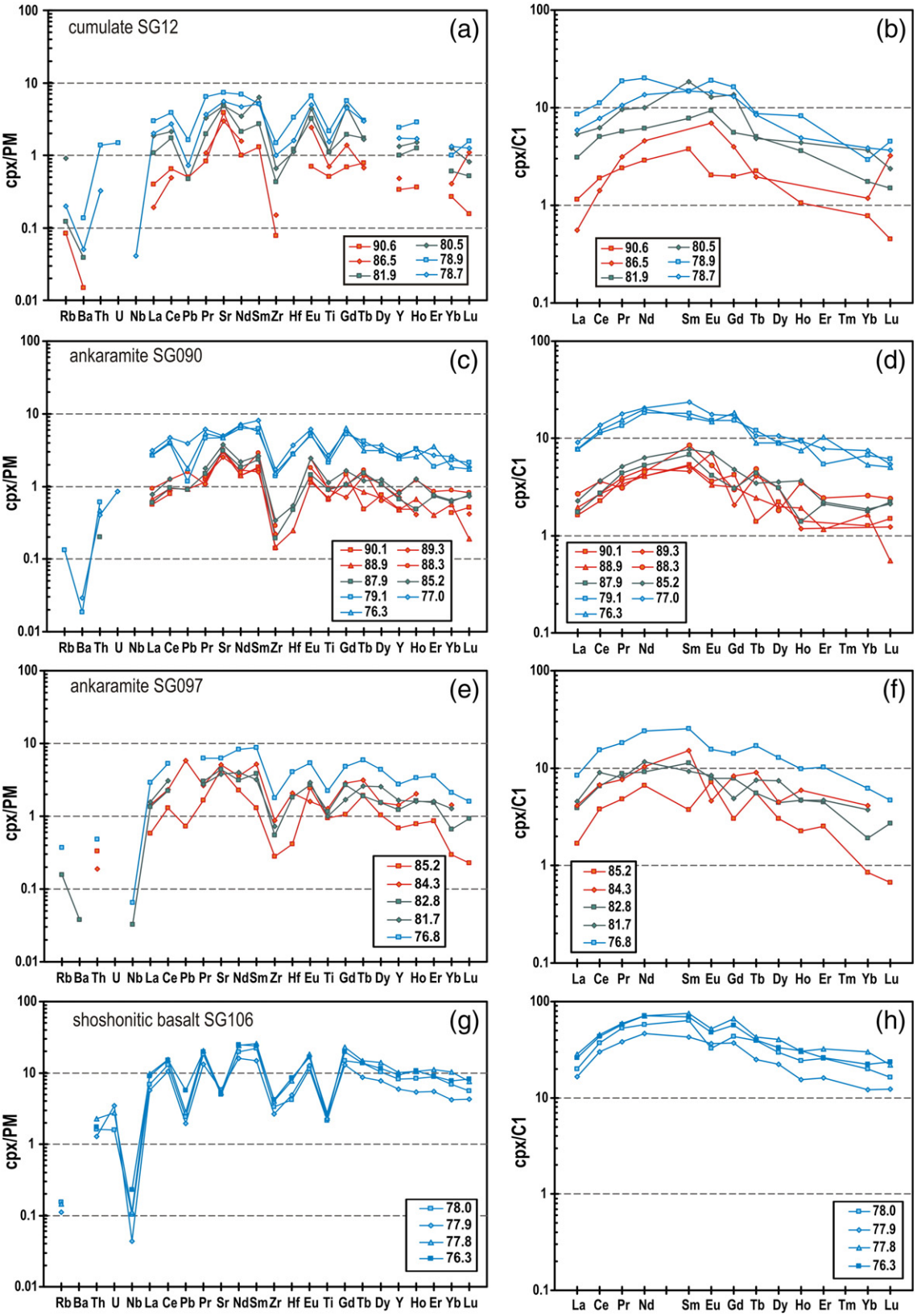

Fig. 4. (a, c, e, g) Primitive mantle-normalized trace element patterns and (b, d. f, h) chondrite-normalized REE patterns for clinopyroxene from the Yambol–Burgas mafic rocks. Data source from Table 6 in the Appendix. Normalizing values from Sun and McDonough (1989). Digits in the legend mean Mg# of clinopyroxene.

Trace element composition of bulk-rocks, olivine and clinopyroxene phenocrysts and their primary melt inclusions, as well as other phenocrysts were determined by LA-ICPMS in ETH Zurich, using an ArF Excimer UV (193 nm) laser source with an energy homogenized beam profile coupled with an ELAN 6100 ICP quadruple mass spectrometer. The analyses at the University of Perugia were performed using a Thermo Electron X7 quadruple ICPMS coupled to a New Wave UP213 frequency quintupled Nd–YAG laser. LA-ICPMS analyses of the silicate melt inclusions were conducted following the method of Halter et al. (2002). We quantified the composition of the melt inclusions using the method of Zajacz and Halter (2007). Composition of olivine-hosted melt inclusions was calculated based on Fe–Mg exchange equilibrium between olivine and silicate melt. A $Kd_{Fe2+-Mg} = 0.32$ was used based on Ulmer (1989). We estimated an Fe^{2+}/Fe_{tot} ratio of about 0.7 in the silicate melt using the method of Kress and Carmichael (1991) and the estimated oxygen fugacities (see below) and used this value to calculate the Fe^{2+} content of the melt. Good textural evidence for the cotectic crystallization of olivine and clinopyroxene allowed us to use the assumption that the CaO/Al_2O_3 ratio in the clinopyroxene-hosted melt inclusions should correspond to those analyzed in olivine-hosted melt inclusions. An average value of $CaO/Al_2O_3 = 1.26$ was used to determine the appropriate amount of host clinopyroxene subtraction from the mixed ablation signals. This analytical approach allows determination of the composition of the bulk melt inclusion including the host mineral that crystallized on the walls of the melt inclusion after entrapment. For further details of the analytical and quantification approach the reader is referred to Zajacz and Halter (2007).

4. Petrography and mineralogy

Ankaramites and absarokites are highly porphyritic with clinopyroxene and olivine as the only phenocrysts along with minor spinel inclusions and microphenocrysts of spinel and Ti-magnetite. The cumulitic nature of SG12 is strongly suggested by the abundant (78 vol.%) phenocrysts (Fig. 2a), represented by approximately equal amount of olivine (39 vol.%) and clinopyroxene (39.4 vol.%). Abundant plagioclase joins these phases in the shoshonitic (high-alumina) basalts, accompanied by phenocrysts of Ti-magnetite and apatite. The phenocrysts in the most magnesian ankaramites and cumulitic lavas reach up to 1.5 cm in size. They become smaller with decreasing MgO content in the absarokites and shoshonitic basalts. The phenocrysts of SG12 are included in a glassy groundmass totally replaced by chlorite with tiny biotite, plagioclase, K-feldspar, apatite needles and altered glass. Chlorite, calcite and quartz are present in the groundmass, amygdales and rarely in veinlets of the ankaramites. The groundmass of the least altered absarokite samples consists dominantly of plagioclase, pyroxene, magnetite and analcite. Shoshonitic basalts are glassy to microcrystalline and holocrystalline in some subvolcanic bodies (e.g. SG27).

4.1. Mineral chemistry

4.1.1. Major element chemistry

Olivine phenocrysts are preserved only in the cumulitic rock SG12. Representative major element compositions of olivine from the rock are presented in Table 2 in the Appendix. In the other mafic rocks they are totally replaced by talc, calcite and chlorite. Olivine crystals in SG12 are large with rare megacrysts up to 1.5 cm in size (Fig. 2a) showing minor to moderate hydration along cracks (Fig. 2b). No deformation textures, such as kink banding or undulose extinction, have been observed in the crystals. Olivine is typically Mg-rich, with broad central region of Fo_{91-87} composition and thin rim reaching Fo_{85-86} (Tables 1 and 2 in the Appendix). The CaO content of the olivine is in the range of 0.53–0.38 wt.%, determined by LA and WDS analyses, much higher than those of typical subduction-related magmas (0.25–0.15 wt.%; Sigurdsson et al., 1993; Smith and Leeman, 2005). The overall high-CaO contents of the olivine could be explained by the crystallization from high-Ca (ankaramitic) magmas (Beattie, 1993). Alternatively, the higher CaO content of the olivine may be due to the high alkali concentrations in the melts, as Na_2O raises Ca partitioning coefficients between olivine and melts (Libourel, 1999). The somewhat higher CaO contents in the olivine

Table 2
Major element composition and CIPW norm of 18 mafic volcanic rocks from the Yambol–Burgas region.

Sample	Cumulate	Ankaramites					Absarokites			Shoshonitic basalts								
	SG12	SG090	SG090*	SG090a	SG097	SG097*	SG21	SG095	SG102a	SG096a	SG094	SG094b	SG086	SG25	SG26	SG087	SG27	SG106
SiO_2	43.91	47.85	45.87	46.28	47.35	47.79	47.71	52.73	50.64	50.20	50.81	52.80	49.76	51.10	51.45	50.92	51.54	50.37
TiO_2	0.26	0.61	0.53	0.63	0.73	0.68	0.71	0.61	0.63	0.87	0.81	0.71	0.70	0.70	0.71	0.68	0.65	0.66
Al_2O_3	4.34	10.73	9.77	11.69	10.43	10.99	12.86	12.82	11.72	14.09	16.32	17.08	15.96	17.09	16.70	17.31	17.66	16.05
Fe_2O_3	6.69	10.05	9.98	11.06	10.33	10.98	6.27	9.49	9.22	11.54	7.83	8.27	8.35	4.76	2.97	8.09	4.24	8.18
FeO	5.12						3.63							2.56	4.65		3.05	
MnO	0.22	0.17	0.16	0.18	0.17	0.16	0.16	0.16	0.15	0.19	0.15	0.16	0.19	0.17	0.17	0.17	0.16	0.18
MgO	24.39	11.06	11.43	9.66	7.78	7.69	6.85	7.10	8.98	5.20	3.93	3.84	3.72	4.20	3.58	3.86	3.94	3.52
CaO	7.72	12.96	14.83	11.42	12.76	12.44	11.88	8.03	10.53	7.52	6.12	6.42	8.16	7.65	7.65	6.32	6.70	6.12
Na_2O	0.14	1.55	1.55	1.02	1.91	2.09	0.62	2.23	1.78	2.16	2.11	2.44	4.13	2.83	3.78	4.35	4.02	3.97
K_2O	0.29	1.77	1.35	3.15	3.04	2.83	5.35	4.72	4.33	5.30	7.29	5.63	3.77	4.45	4.08	3.75	3.48	5.41
P_2O_5	0.13	0.26	0.21	0.32	0.39	0.39	0.25	0.37	0.43	0.54	0.44	0.33	0.49	0.39	0.40	0.48	0.42	0.47
LOI	6.79	2.47	3.45	5.29	5.08	3.45	3.71	1.63	1.22	1.54	3.69	1.32	4.76	4.11	3.86	3.94	4.13	4.61
SO_3		0.02		0.03	0.01				0.02		0.01		0.06			0.07		
Total	100.00	99.48	99.13	100.70	99.97	99.48	100.00	99.89	99.63	99.13	99.51	98.99	100.00	100.01	100.00	99.88	99.99	99.56
Mg#	82.1	71.9	72.7	67.1	63.7	62.0	60.8	63.5	69.4	51.2	53.9	52.0	50.9	56.3	50.6	52.6	54.6	50.1
CaO/Al_2O_3	1.78	1.21	1.52	0.98	1.22	1.13	0.92	0.63	0.90	0.53	0.38	0.38	0.51	0.45	0.46	0.37	0.38	0.38
Or	1.85	10.88	19.71	8.42	19.11	17.58	22.23	28.63	26.21	32.40	45.28	34.33	23.57	27.53	25.13	23.27	21.52	33.89
Ab	1.28	11.19	5.44	3.02	5.90	8.42		19.39	9.36	14.45	7.99	21.26	20.14	22.18	23.70	27.83	30.64	16.74
An	11.17	17.77	19.07	16.54	11.60	12.89	17.22	11.30	11.47	13.58	14.22	19.62	14.68	21.76	17.24	17.46	20.79	10.62
Ne		1.33	2.00	5.88	6.12	5.49	2.97		3.29	2.40	5.84		9.12	1.56	5.22	5.86	2.68	10.25
Di	23.33	38.24	31.47	48.09	43.29	40.41	34.90	22.10	31.74	17.75	12.12	9.15	20.56	12.61	16.26	10.08	9.19	15.22
Hy	26.34							1.78				1.19						
Ol	32.31	16.54	17.76	14.25	9.21	10.46	9.93	12.63	13.68	13.85	10.09	10.43	7.43	10.31	8.26	11.15	11.14	8.90
Mt	2.90	2.27	2.55	2.29	2.39	2.51	2.34	2.12	2.05	2.60	1.79	1.85	1.92	1.73	1.84	1.85	1.74	1.89
Il	0.53	1.20	1.27	1.06	1.48	1.35	1.41	1.19	1.23	1.70	1.62	1.39	1.41	1.39	1.41	1.36	1.29	1.33
Ap	0.32	0.63	0.79	0.52	0.96	0.94	0.60	0.89	1.02	1.30	1.07	0.78	1.20	0.95	0.97	1.17	1.02	1.17
Lc							8.44											

Mg# and CIPW norm calculated at $Fe_2O_3/FeO_T = 0.15$.
Samples SG12, SG21, SG25, SG26, SG27 — analyzed in Florence, samples SG090*, SG097*, SG095, SG096a, SG94b — analyzed in Lausanne, other samples from Georgiev (2008).

cores (0.53–0.41) compared to the rims (0.41–0.38) may be a reflection of the higher Ca content in the melt at the early crystallization of the olivine core and the decreases of Ca content after the clinopyroxene joined olivine crystallization. Alternatively, it could be simply a reflection of decreasing crystallization temperature as suggested by Jurewicz and Watson (1988).

Clinopyroxene phenocrysts are fresh and optically and chemically zoned (Table 3 in the Appendix). Clinopyroxene in the ankaramites (SG090, SG097) and cumulate SG12 forms large (up to 10 mm) crystals and glomerocrysts. They commonly have a corroded and sieved zoned high-Mg core (Mg# 91–87), followed by oscillatory outer zone (Mg# 85–72) and very thin rim of Mg#66–69 (Fig. 2c, d). The Mg# of clinopyroxene in the absarokites and shoshonites varies between 89.5 and 76. Microlites of all rocks are less Mg-rich (Mg# 65–68), similar to the outermost rims of the clinopyroxene phenocrysts. The presence of microlites of high-Fe (Mg#49), high-Mn (up to 2.5 wt.%) and high Na (up to 1.0 wt.%) in the shoshonitic basalts SG27 (an. 38) is noteworthy. The Mg# of the clinopyroxenes shows strong negative correlation with TiO_2 and Al_2O_3 and positive correlation with Cr_2O_3.

Spinel occurs as small inclusions (up to 100 μm) in the olivine phenocrysts or as microphenocrysts in the cumulate, ankaramites and absarokites. Analyses from the cumulate SG12 and absarokite SG095 are given in Table 4 in the Appendix. The Cr-numbers [$Cr\# = 100 \times Cr/(Cr + Al)$ mol] of the spinels enclosed in the high-Fo (~90) olivine of the cumulate SG12 are higher (75–78) than those in the microphenocrysts (65–67) and the spinels from the less magnesium (~Fo_{85}) outer rims (Cr#67–70). A similar correlation is recorded also in the Mg#, Fe^{2+}/Fe^{3+} ratios and the Al_2O_3 contents. On the contrary, TiO_2 contents increase from the core (0.40–0.60 wt.%) trough the rim (1.02–1.13 wt.%) and in the microphenocrysts (1.40–1.52 wt.%). Spinels included in altered olivines of the absarokite SG095 have similar compositions to those in the olivine cores of the cumulate SG12. The TiO_2 vs. Al_2O_3 contents of the spinels falls within the array of calc-alkaline and high-K volcanic arc spinel of Kamenetsky et al. (2001) (Fig. 3a). The spinels included in the high-Fo cores fall within the olivine–spinel mantle array (Fig. 3b) defined by Arai (1994), whereas the rim spinel–olivine pairs fall outside this array, exhibiting a trend with slightly negative slope. Such a trend most probably results from crystallization of olivine and clinopyroxene, which is consistent also with the decrease of the CaO/Al_2O_3 ratio in the melt inclusions (see below).

Ti-magnetite forms microphenocrysts in most mafic cumulates, ankaramites and absarokites and large (up to 0.8 mm) crystals in the shoshonitic basalts (Fig. 2e). Ulvöspinel content varies from 8.5 to 19.4 wt.%. A tendency of increase of MgO (0.4–5.2 wt.%) and decrease of Al_2O_3 (0.8–8.0 wt.%) is recorded in the transition from the core to the rim and microlites. Negligible amounts of Zn (<0.1 wt.%) and Ni (~0.1 wt.%) have been detected in Ti-magnetite of the cumulate and ankaramite samples.

Apatite occurs as needle-like inclusions in clinopyroxenes in most mafic rocks or as large (up to 0.8 mm) phenocrysts in shoshonitic basalts (Fig. 2e).

Biotite in SG12 occurs as microlites less than 100 μm with variable composition (not shown). Mg# varies from 54.2 to 71.1; TiO_2 content is in the range of 1.6–3.2 wt.%. Fluorine content varies between 0.7 and 1.0 wt.%, and the Cl concentration is below 0.1 wt.%. Groundmass in the Rudnik shoshonitic basalt contains quenched crystals of biotite (Mg#64.4).

Plagioclase (Table 5 in the Appendix) forms microphenocrysts in the absarokite SG102a with a compositional range of An_{60-50}. Plagioclase microlites and mesostasis have compositions of An_{46} and An_{20}, respectively. The compositional range of the plagioclase phenocrysts from the shoshonitic basalts SG25 is $An_{72.7-55.5}$.

K-feldspar. Replacement of the sieved zoned cores of plagioclase by sanidine (Or_{61-85}), compositionally similar to the sanidine microlites (Or_{59-53}) is typical for the shoshonitic basalts. Sanidine microlites (Or_{95}) are also present in the groundmass of the absarokite SG095.

Analcite occurs in the mesostasis or as microlites in the groundmass of the absarokite SG095 (Fig. 2f).

4.1.2. Trace element composition of olivine and clinopyroxene

Representative analyses of 5 olivine and 25 clinopyroxene crystals are shown in Table 1 in the text and Table 6 in the Appendix, respectively.

Olivine in SG12 has very low-Ni concentrations, exhibiting also a slight decrease from the high-Mg (Fo_{90}) core (1100–1140 ppm) to Fo_{85} rim (~1050 ppm). Similar low-Ni counterparts to the Eastern Srednogorie cumulitic olivines have been reported from Western Epi, Vanuatu (Barsdell and Berry, 1990); high-Ca olivines from Mg-rich magmas from South Sulavesi (Elburg et al., 2006) and medium-K ankaramites from Lombock, Indonesia (Elburg et al., 2007). A similar zoning pattern is even more prominent for Cr (>300 ppm in the core and ~170 ppm in the rim).

Clinopyroxene. Fig. 4 shows primitive mantle-normalized trace element and chondrite-normalized rare earth element (REE) patterns of clinopyroxenes from the cumulate SG12, ankaramites, absarokites and shoshonitic basalts. Trace- and REE concentrations show pronounced negative correlation with the Mg# of the clinopyroxenes. All clinopyroxenes are relatively depleted in high field strength elements (HFSE) Ti, Zr, Nb and Hf. Large ion lithophile elements (LILE) Rb, except for Th and U, are depleted with particularly deep troughs in Ba and Pb. Sr shows a positive anomaly in the most Mg-rich zones of the clinopyroxene and negative anomalies in the less Mg-rich outer rims and zones of the cumulate SG12 and ankaramites. In contrast, the shoshonitic basalts have a pronounced negative Sr anomaly. Chondrite-normalized REE patterns are convex-upward, peaking at Nd and Sm. The concentrations are 0.5 to 25 times higher relative to chondrite values in

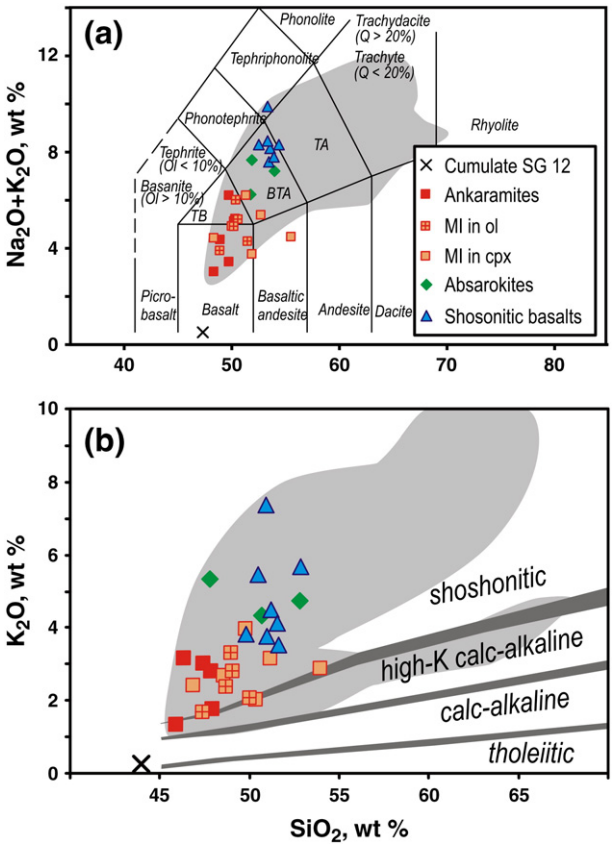

Fig. 5. Classification diagrams for the mafic rocks from the Yambol–Burgas region and melt inclusions (MI) in the olivine and clinopyroxene from cumulate SG12, compared to the composition of the rocks from the entire region (gray field). (a) Total alkali-silica (TAS), fields from Le Maitre et al. (2002); and (b) K_2O vs. SiO_2 (Rickwood, 1989). Data for the rocks from the region is from Georgiev (2008). Major element data in TAS diagram are on an anhydrous 100% adjusted basis, whereas in K_2O vs. SiO_2 are with LOI.

Table 3
Trace element composition of studied mafic rocks from the Yambol–Burgas region.

Sample	Cumulate	Ankaramites					Absarokites			Shoshonitic basalts								
	SG12	SG090	SG090*	SG090a	SG097	SG097*	SG21	SG095	SG102a	SG096a	SG094	SG094b	SG086	SG25	SG26	SG087	SG27	SG106
Sc		44	30	37	35	13		14	29	11	18	5	17			16		18
V	106	249	227	264	238	241	291	228	208	294	255	254	263	249	257	245	242	257
Cr	1900	565	544	438	397	282	288	242	367	91	119	10	133	26	31	100	27	43
Co	96	40	52	43	37	46	38	30	36	33	23	22	22	23	26	21	26	21
Ni	531	106	96	84	97	64	61	62	98	38	52	8	42			29		22
Cu	30	98	81	93	38	51	103	88	46	120	119	139	175	96	103	134	130	86
Zn	72	59	64	63	65	72	68	76	87	97	63	73	74	93	93	82	111	73
Rb	15	34	36	63	43	41	78	148	122	131	153	132	84	82	101	96	82	99
Sr	87	598	341	678	696	746	383	598	1098	1315	2226	6201	820	845	1148	1193	947	869
Y	7	13.1	16	13.2	14.5	18	17	23	13.8	26	22.4	25	19.8	20	21	19.1	19	19.5
Zr	24	31	36	39	54	75	48	76	86	123	92	139	77	71	72	77	69	76
Nb	bdl	1.23	3	1.54	1.95	4	1	8	3.02	5	3.57	bdl	3.55	1	3	3.13	3	3.52
Cs		0.17		2.64	0.22				6.40		0.65		1.43			2.29		2.34
Ba	69	130	149	218	400	368	372	450	497	648	429	431	364	432	423	389	401	533
La	4	9.80	17	13.19	13.17	10	19	37	24.91	33	20.83	25	20.96	22	24	19.73	20	19.50
Ce	5	20.52	31	25.76	28.13	33	36	45	49.58	79	45.61	65	42.95	51	58	42.28	49	43.23
Pr		2.66		3.36	3.63				5.98		5.71		5.14			5.03		5.56
Nd	2	14.07	18	14.49	16.77	15	19	27	27.88	41	27.45	30	25.12	30	31	24.93	28	24.37
Sm		3.69		3.71	4.18				5.46		5.20		5.00			5.15		5.51
Eu		0.92		1.13	1.12				1.49		1.70		1.31			1.65		1.66
Gd		2.60		2.92	4.00				4.58		5.16		5.26			4.51		4.76
Tb		0.37		0.48	0.54				0.64		0.65		0.71			0.65		0.60
Dy		2.11		2.55	2.71				2.69		3.90		3.07			3.50		3.45
Ho		0.49		0.42	0.45				0.48		0.55		0.62			0.59		0.71
Er		1.20		1.27	0.99				1.25		2.61		1.77			1.76		1.99
Tm		0.20		0.17	0.17				0.16		0.51		0.29			0.26		0.28
Yb		1.00		1.44	1.30				1.33		3.18		2.27			1.66		1.96
Lu		0.11		0.22	0.30				0.20		0.32		0.25			0.23		0.25
Hf		0.85		0.84	1.33				2.11		3.05		1.79			2.20		1.75
Ta				0.14	0.20				0.24		0.52		0.31			0.29		0.35
Pb	bdl	6.88	bdl	8.16	4.96	3	13	12	15.13	16	9.34	24	18.63	27	26	23.21	19	16.97
Th	bdl	2.10	bdl	2.92	2.84	bdl	2	8	10.08	4	7.09	bdl	7.89	9	6	6.89	8	7.57
U	1	0.63	2	0.88	0.85	2	1	3	3.93	bdl	3.81	bdl	4.66	1	2	4.09	1	2.49
Eu/Eu*		0.90		1.05	0.83				0.91		1.00		0.78			1.05		0.99
$(La/Yb)_N$		7.01		6.59	7.29				13.47		4.71		6.62			8.52		7.14

bdl — below detection limit. Samples SG12, SG25, SG26, SG27, SG21 — analyzed in Florence, samples SG090*, SG097*, SG095, SG096a, SG94b — analyzed in Lausanne, all other samples from Georgiev (2008).

the cumulate and ankaramite (Fig. 4). The enrichment levels of the shoshonitic basalts are much higher (12 to 75 times chondrite). Most clinopyroxenes from the cumulate and ankaramites lack Eu anomalies (Eu/Eu* = 0.9–1.2) unlike those from the shoshonitic basalts, which show appreciable Eu anomalies (Eu/Eu* = 0.7–0.9). La/Yb_n values vary between 0.5 and 3.0 with most being in the range of 1–1.4.

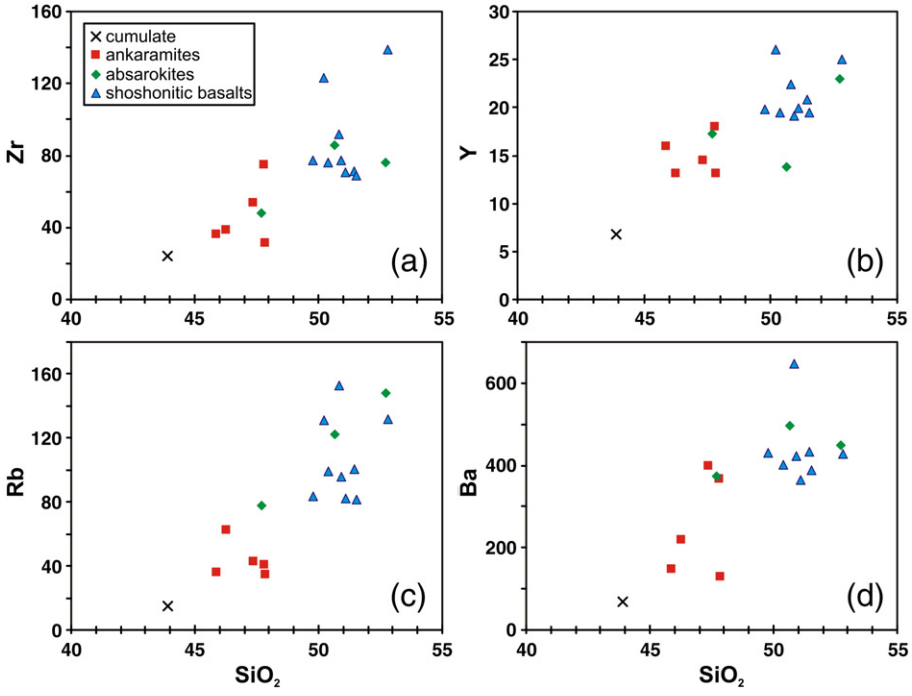

Fig. 6. Variation diagrams for, Zr, Y, Rb and Ba (ppm) vs. SiO_2 (wt.%) for the mafic rocks from Yambol–Burgas region.

5. Major, trace element and isotopic composition of mafic magmas

5.1. Major element composition

The major element composition of 18 mafic lavas and dykes discussed in this study are given in Table 2 and compared with the entire rock collection of Georgiev (2008) from the Yambol–Burgas region in Fig. 5a and b. The volcanic rocks have been variably affected by low-grade (propylitic) alteration, as suggested by the secondary mineral assemblages and their LOI varying between 1.2 and 6.8 wt.%. However, our comparison with the melt inclusion chemistry (see below) shows that the alteration did not affect significantly the rock compositions except for the samples with K_2O/Na_2O ratio >> 2 (e.g. SG21), which were taken from the interior of pillow lavas. These samples are characterized by progressive replacement of the groundmass by K-feldspar. In the K_2O–SiO_2 diagram of Rickwood (1989), mafic rocks from the Yambol–Burgas region plot in the fields of the shoshonitic ($K_2O/Na_2O = 1–2$) and ultrapotassic ($K_2O/Na_2O > 2$) varieties, whereas in the TAS diagram (Le Maitre et al., 2002) they fall in the fields of basalts, trachybasalts and basaltic trachyandesites. Throughout the paper, however, we follow our petrographic division into cumulates, ankaramites, absarokites and shoshonitic basalts.

The cumulitic sample SG12 has a very unusual major element composition with very low SiO_2 (~44 wt.%), high MgO (24.4 wt.%) and FeO (11.2 wt.%) and very low Na_2O (0.14 wt.%) and K_2O (0.29 wt.%). Calculated Mg# of this rock (assuming $Fe_2O_3/FeOt = 0.15$) is 82.1, while the CaO/Al_2O_3 is 1.78. This composition is much more primitive than its high-Mg olivine- and clinopyroxene-hosted melt inclusions (see below), strongly suggesting that the whole rock composition is the result of accumulation of olivine, clinopyroxene and spinel (see below). Ankaramites have 45.9–47.9 wt.% SiO_2, 6.9–11.4 wt.% MgO and CaO/Al_2O_3 of 0.98–1.52. Absarokites have higher SiO_2 (50.6–52.7 wt.%), lower MgO (7.1–8.9 wt.%) and lower CaO/Al_2O_3 ratios (0.63–0.90). Compared to the absarokites, shoshonitic basalts have similar SiO_2 (50.2–52.8 wt.%), but much lower MgO (3.5–4.2 wt.%) and CaO/Al_2O_3 ratios (0.37–0.53). All of them, except SG095 and SG094b, are nepheline-normative with Mg # decreasing from the ankaramites and absarokites (60.8–72.7) to the shoshonitic basalts (50.1–56.3).

5.2. Trace element composition

Trace element composition of the Yambol–Burgas mafic magmas is reported in Table 3. Consistent with its cumulitic nature, sample SG12 has very high Ni and Cr contents, 530 ppm and 1900 ppm, respectively. The concentration of these elements is also high in the ankaramites and decreases towards the absarokites and the shoshonitic basalts showing co-variations with MgO rather than SiO_2. It is noteworthy, that even the most mafic ankaramites have low Ni (~100 ppm) at high Cr (>400 ppm). Similar chemical features have been reported for the high-K ankaramite-like rocks from Lihir Island, Papua New Guinea (Kennedy et al., 1990).

Most of the incompatible trace elements increase with increasing SiO_2 contents as represented by Zr, Y, Rb and Ba (Fig. 6). Interestingly, several more potassium rich samples (e.g. SG094; SG094b) have very high Sr values (2200–6200 ppm) at comparatively low Ba concentrations (360–420 ppm).

The primitive mantle-normalized trace element patterns (Fig. 7a) show uniform characteristics in the 3 rock types with peaks in LILE (Rb, U, Pb, Sr) and troughs in Nb, Ta, Ti and Hf which are all typical features of subduction-related magmas. While the overall patterns are similar, the relative trace element abundance in the ankaramites is lower than that in the absarokites and the shoshonitic basalts.

Chondrite-normalized REE patterns (Fig. 7b) display a pronounced enrichment of light REE relative to heavy REE resulting in La/Yb_n ratios from 4.7 to 13.5. The overall REE abundance and the La/Yb_n ratio increase from the ankaramites towards the more evolved absarokites and shoshonitic basalts. The HREE patterns of the ankaramites show some troughs and spikes and an unusual profile of the ultrapotassic sample SG094, which seem to reflect inaccuracy of measurements. This obscures a correct evaluation of the slope of HREE in the ankaramites as an indicator for the presence or absence of garnet in the source.

6. Melt inclusions

6.1. Melt inclusion description

Melt inclusions are observed in both olivines and clinopyroxenes from the cumulitic sample SG12. The melt inclusions are usually rare; their shape varies from rounded through ellipsoidal to negative crystal forms (Fig. 8a, b, d, e). The inclusions generally consist of a colourless glass and a shrinkage bubble. Rarely, they contain spinel inclusions (Fig. 8a). The diameter of the melt inclusions range from a few up to ~40 μm. Some melt inclusions show minor post-entrapment crystallization. Trails of small melt inclusions, occurring along healed fractures, have been rarely observed (Fig. 8b, c).

6.2. Major elements

Electron microprobe and LA-ICPMS data on the melt inclusions are shown in Table 4 and compared with the whole rock compositions in Fig. 5a and b. Uncorrected (with no host addition to compensate post-

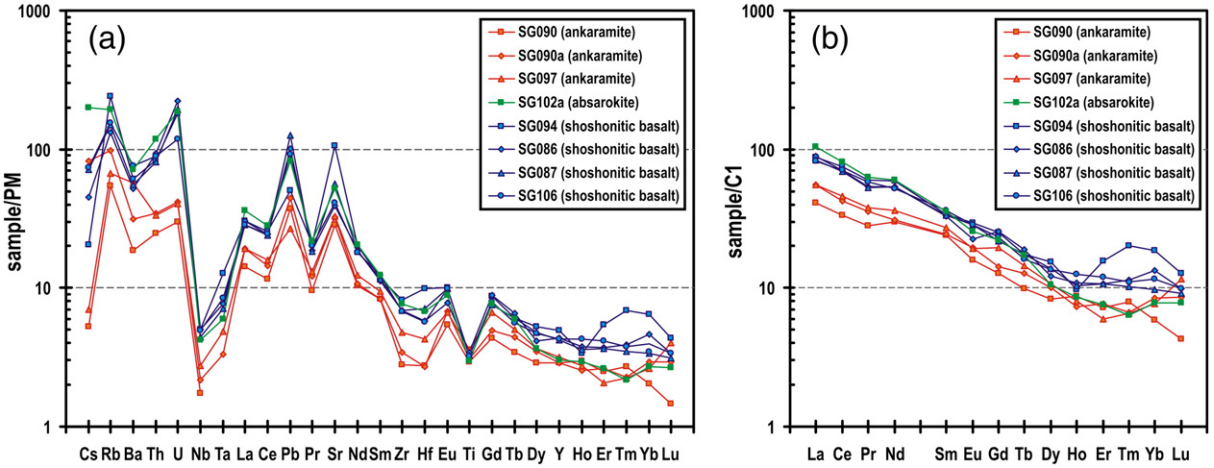

Fig. 7. (a) Primitive mantle-normalized trace element patterns and (b) chondrite-normalized REE patterns for Yambol–Burgas representative mafic rocks. The data source from Table 3. Normalizing values from Sun and McDonough (1989).

entrapment crystallization) EPMA analyses of the inclusions hosted in the high-Fo_{90-91} olivine cores show $SiO_2 = 52–53$ wt.%, $Al_2O_3 \sim 16.0$ wt.%, very low MgO (~1 wt.%) and FeO (~3 wt.%), with no essential difference between defocused (5 μm) and spot analyses. Na_2O and K_2O vary between 2.1–2.6 wt.% and 2.9–3.7 wt.%, respectively, with the higher values recorded in the defocused analyses. Compared to the core-melt inclusion compositions, analyses of a melt inclusion in a low-Fo_{85} olivine rim exhibits similar SiO_2 content, lower MgO, FeO and CaO, but higher Al_2O_3, Na_2O and K_2O contents.

Melt inclusions in olivine and clinopyroxene phenocrysts, analyzed by LA-ICPMS using the method of Halter et al. (2002) exhibit lower SiO_2 (47.5–51 wt.%), except for one analysis in clinopyroxene (54.0 wt.%), lower Al_2O_3 (10–12 wt.%) and lower alkalis. MgO, FeO and, to a lesser extent, CaO show much higher values, compared to the defocused EPMA analyses: (7.5–10.8 wt.% MgO, 6.5–10.7 wt.% FeO and 11.9–15.0 wt.% CaO). This is due to the fact that this method compensates for the post-entrapment crystallization of the host mineral on the walls of the inclusion. Overall, the melt inclusion compositions are characterized by marked enrichment in K_2O (~2–3 wt.%) and K_2O/Na_2O ratio varying between 0.8 and 1.25 with most values around unity. Based on their high-CaO/Al_2O_3 and K_2O/Na_2O ratios, the chemical composition of the melt inclusion in SG12 can be classified as being both ankaramitic and shoshonitic.

6.3. Trace element composition

Comparison between trace element data from entirely ablated (Zurich) melt inclusions and corrected to $SiO_2 = 48$ wt.% melt inclusion measured in Perugia (Table 5, an. 6) shows identical values for all element of melt inclusions hosted in high-Fo_{90-91} olivines. In Fig. 9, the primitive mantle-normalized trace element and chondrite-normalized REE patterns of melt inclusions hosted in olivines and clinopyroxenes are compared with those of whole rock ankaramites. In general, the melt inclusions display strong resemblances to the lavas,

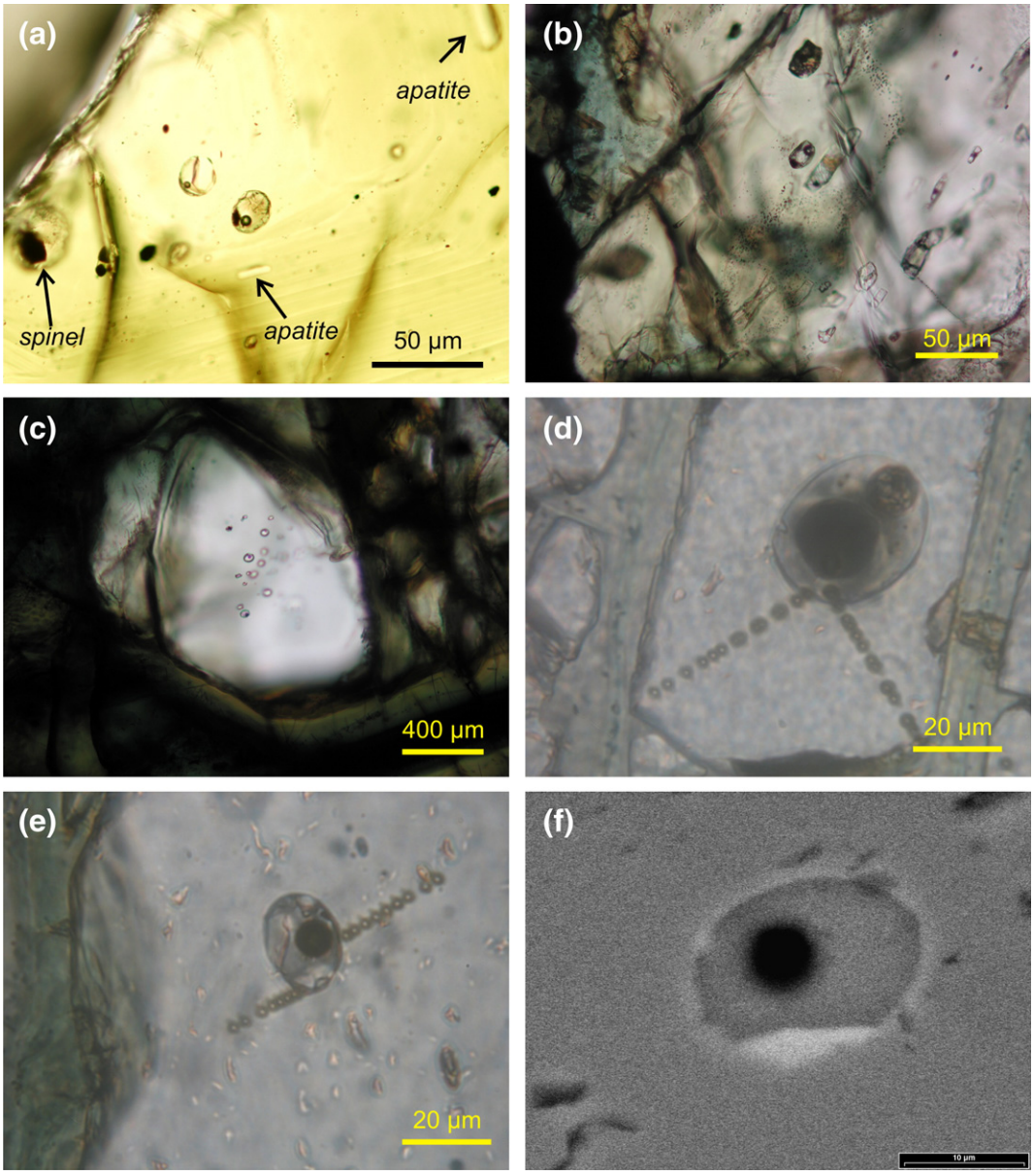

Fig. 8. Melt inclusions in the olivine of cumulate SG12; all images except (f) are transmitted-light photomicrographs. (a) Ellipsoidal and rounded MIs, mostly two phase (glass and shrinkage bubbles). The right one contains small crystallites and spinel. Note apatite crystals oriented parallel to crystal growth. (b, c) Trails of secondary melt inclusions. (d) High-resolution profiles (2–3 μm steps) from 42 μm glass–fluid melt inclusion located into the core of an olivine crystal (Fo_{91}). (e) High-resolution profiles (2–3 μm steps) from 20 μm glass–fluid melt inclusion located into the rim of an olivine crystal (Fo_{85}). (f) Back-scattered SEM image of the same melt inclusion. The lighter zone around the melt inclusion shows enrichment in Fe close to host olivine.

Table 4
Electron microprobe and LA-ICPMS analyses for melt inclusions in olivine from the cumulitic rock SG12.

	1	2	3	4	5	6	7	8	9
	EPMA			LA-ICPMS			EPMA		LA-ICPMS
	5 μm	5 μm	1 μm	jn27a15	jn27a17	jn27b06	5 μm	5 μm	au28a05
SiO_2	50.86	51.9	53.16	49.06	48.68	49.98	51.36	51.96	48.95
TiO_2	0.97	1.07	1.15	0.63	0.5	0.39	1.15	0.91	0.64
Al_2O_3	16.04	15.84	16.15	12.86	12.27	11.20	18.36	18.98	14.87
FeO	3.28	3.11	3.27	6.44	7.63	8.72	2.29	1.69	6.96
MnO	0.1	0.05	0	0.11	0.1	0.14	0.05	0.16	0.13
MgO	1.01	0.95	0.97	8.00	9.29	7.45	0.73	0.5	5.2
CaO	16.72	17.61	16.34	14.90	13.77	14.97	14.34	13.2	14.53
Na_2O	2.84	2.61	2.13	2.22	2.41	2.11	2.99	3.03	2.53
K_2O	3.17	3.66	2.89	2.78	2.35	2.04	3.35	4.1	3.28
P_2O_5	0.71						0.97	1.41	
SO_3	0.07							0.72	
F	0						0.25	0.16	
Cl	0.19						0.2	0.24	
H_2O				3.00	3.00	3.00			3.00
Ni				164.00					210
Cr				302.00	364.00				134
Total	94.99	96.80	96.06	100.00	100.00	96.04	96.04	97.06	100.09
Fo	90.4	90.4	90.4	90.80	90.6	87.2	84.9	84.9	84.9

an. 1, 2 — quenched residual melt of 42 μm melt inclusion in the core ($Fo_{90.4–90.8}$); 4–6 LA-ICPMS analyses using the method of Halter et al. (2002); an. 7–8 quenched residual melt of 20 μm melt inclusion in the rim ($Fo_{84.9–85.1}$); an. 9 LA-ICPMS of the same inclusion. Given is the beam size in μm.

with pronounced negative anomalies for Nb, Ta, Zr, Hf, Ti and Ba, and spikes for Rb, Th, Pb and Sr (Fig. 9a, c), although with much larger variations in the melt inclusions. The chondrite-normalized REE patterns of the melt inclusions and ankaramites (Fig. 9b, d) are also similar. One olivine-hosted melt inclusion (#3), which has the lowest K_2O content, has aberrant trace element patterns with very low light and heavy REE at MREE similar to other melt inclusions. One clear difference is the depletion of Er, Tm and Yb in all high-Fo melt inclusions. If these values are real, they lead to steep HREE fractionation (Tb_n/Yb_n ratio > 1.5) consistent with melting in the garnet stability field. However, our preferred interpretation is that the steeper HREE patterns are the result of a higher diffusion rate of these elements through the olivine, as suggested by Spandler et al. (2007).

6.4. Volatile elements

6.4.1. H_2O

There is no direct determination of H_2O in the studied melt inclusions. However, the total of most electron microprobe analyses is between 95 and 98 wt.%, which indicates that the glasses contain ~3 wt.% H_2O. This value is close to the results obtained by Gioncada et al. (1998) for the melt inclusions in the most mafic magmas from Volcano Island (Aeolian Islands), which are compositionally the closest match to our ankaramitic melt inclusion compositions. Using SIMS and FTIR analyses, these authors obtained H_2O contents between 1.8 and 2.9, and 2.1 and 3.8 wt.%, respectively. Additional support to our conclusion that the Srednogorie ankaramite magma was water-rich initially arises from the experimental studies of Gaetani and Grove (1998) demonstrating that the hydrous partial melting of peridotite produces liquids with elevated $SiO_2/(MgO + FeO)$ ratios of >2.3. Four of the olivine-hosted melt inclusions in SG12 display $SiO_2/(MgO + FeO)$ ratios of 2.19 to 3.18, with 3 of them exceeding 2.88. Surprisingly, similar ankaramitic magmas from South Sulawesi (Elburg et al., 2006) have considerably lower H_2O contents (0.5–0.8 wt.%), which these authors interpreted as the result of water loss.

6.4.2. Chlorine, fluorine, lithium and boron

Chlorine analyses by electron microprobe in two olivine-hosted melt inclusions yielded 0.19–0.24 wt.%. Fluorine content in a single melt inclusion in Fo_{85} varies between 0.16 and 0.25 wt.% (Table 4). Lithium contents in the SG12 olivine- and clinopyroxene-hosted inclusions (Table 5) vary between 5 and 15 ppm, with slightly higher values in the olivine-hosted melt inclusions. Boron concentrations in the measured melt inclusions vary between 6 and 40 ppm.

7. Temperature and oxygen fugacity

The crystallization temperature of the cumulitic sample SG12 has been assessed with a range of thermometers. The magmatic temperature was calculated using olivine–liquid thermometers of Putirka (1997), Putirka et al. (2007 eq.4), Beattie (1993) and Langmuir et al. (1992) (Table 6). For this purpose, we used bulk melt inclusion compositions that were already corrected for the post-entrapment crystallization of the host mineral on the walls of the inclusions. The resulting temperatures for high-Fo core-melt inclusion pairs from sample SG12 range between 1146 and 1266 °C with the lowest temperatures obtained with the Langmuir et al. (1992) and Putirka et al. (2007) thermometers, and the highest temperatures obtained with those of Putirka (1997) and Beattie (1993), respectively. A pressure of 0.5 and 0.7 GPa is assumed for these calculations (see below), but all methods are fairly insensitive, giving an offset of ~5 °C/0.1 GPa. Similar temperatures to those derived from the thermometers of Putirka (1997) and Beattie (1993) are obtained with the olivine–clinopyroxene thermometer (1217–1256 °C) of Loucks (1996). Adjacent olivine rim (Fo_{85})–melt inclusion pair yielded 50 to 110 °C lower temperatures, showing normal cooling and fractionation. The calculated clinopyroxene saturation temperatures using the equation of Putirka et al. (2003) are in the range of the olivine–liquid geothermometers (1173–1214 °C). This internal consistency could be interpreted as evidence of equilibrium or close to equilibrium crystallization of both minerals.

Lower temperatures were obtained for the cumulate SG12 with the olivine–spinel geothermometer of Ballhaus et al. (1991, 1994). Olivine–spinel pairs from the high-Fo core range from 1093 °C to 1124 °C, whereas the temperatures obtained by olivine–spinel pairs from the rim part are 75–105 °C lower, a difference similar to that obtained from the olivine–melt thermometers. Although the lower temperatures of the olivine–spinel thermometer are, most probably, the result of diffusive re-equilibration, we cannot rule out the possibility that this difference is due to dissolved water. If the dissolved H_2O content was ~3 wt.% (see above), it would depress the liquidus temperatures by ~110 °C (Falloon and Danyushevsky, 2000), which is comparable to the observed difference of 70–100 °C. This assumption is consistent with the fact the those olivine–liquid geothermometers resulted the lowest temperatures that are known to best reproduce experimental results for hydrous magmas (i.e. method of Langmuir et al., 1992 and Putirka et al., 2007).

The crystallization temperatures of the ankaramites SG090 and SG097 have been obtained by the clinopyroxene saturation equation of Putirka et al. (2003), using clinopyroxene–whole rock pairs. Obtained temperatures for the sample SG090 are slightly higher (1230–1259 °C) than those of the cumulate, whereas the temperatures for SG097 (1182–1240 °C) are within the range of the cumulate.

The crystallization pressure for the cumulate and ankaramites was estimated with the clinopyroxene–liquid geobarometer of Putirka et al. (1996, 2003). For sample SG12 clinopyroxene, and the bulk composition of olivine- and clinopyroxene-hosted melt inclusions were used. In all other, non-cumulitic rocks the pressure was calculated, using clinopyroxene–whole rock pairs. Although these determinations are relatively inaccurate, the pressure range calculated for the two rock types is very similar; between 0.5 and 1.4 GPa, with most values between 0.6 and 0.9 GPa. Translated into depth these numbers correspond to ~20–30 km, which is slightly above or near the Moho (27–30 km) in the Eastern Srednogorie zone (Georgiev et al., 2001).

Table 5
LA-ICPMS analyses of individual melt inclusions in olivine and clinopyroxene of SG12.

Olivine	1	σ (%)	2	σ (%)	3	σ (%)	4	σ (%)	5	σ (%)	6	7	σ (%)	8	σ (%)	9	σ (%)	10	σ (%)	11	σ (%)	12	σ (%)
	jn27a15		jn27a17		jn27b04		jn27b06		au28a05			jn27a03		jn27a07		jn27a09		jn27b12		jn27b15		jn27b17	
SiO_2	49.06	2	48.68	6	47.38	9	49.98	5	48.95	2	48.00	51.13	4	49.75	2	53.87	8	46.86	5	48.50	3	50.31	7
TiO_2	0.63	3	0.50	5	0.39	6	0.39	5	0.64	4		0.43	7	0.39	5	0.34	11	0.59	5	0.52	4	0.54	8
Al_2O_3	12.86	3	12.27	3	9.87	3	11.20	3	14.87	3		10.68	4	10.46	5	9.44	6	11.57	5	10.93	5	10.87	5
FeO	6.44	2	7.63	8	10.71	11	8.72	7	6.96	4		7.92	4	8.97	4	7.51	6	10.25	4	9.66	3	8.91	5
MnO	0.11	3	0.10	12	0.13	18	0.14	8	0.13	4		0.16	4	0.15	3	0.12	7	0.18	4	0.21	4	0.18	5
MgO	8.00	16	9.29	30	10.84	38	7.45	29	5.20	22		8.04	7	8.12	7	9.57	12	8.67	8	8.67	6	8.86	10
CaO	14.90	3	13.77	4	13.91	5	14.97	4	14.53	3	15.60	13.45	8	13.18	5	11.89	19	14.58	7	13.76	6	13.70	12
Na_2O	2.22	3	2.41	3	2.10	3	2.11	3	2.53	3		2.06	5	2.02	6	1.47	6	1.89	5	2.07	6	1.63	6
K_2O	2.78	3	2.35	3	1.67	3	2.04	3	3.28	3		3.13	6	3.96	6	2.87	6	2.40	6	2.68	6	2.00	6
H_2O	3.00		3.00		3.00		3.00		3.00			3.00		3.00		3.00		3.00		3.00		3.00	
Total	100.00		100.00		100.00		100.00		100.09			100.00		100.00		100.08		100.00		100.00		100.00	
CaO/Al_2O_3	1.16		1.12		1.40		1.33		0.98			1.26		1.26		1.26		1.26		1.26		1.26	
Mg#	90.8		90.6		87.2		87.2		84.9		90.4	78.9		90.6		86.5		78.7		81.9		80.5	
mf	0.61		0.24		0.15		0.26		0.73			0.36		0.50		0.23		0.34		0.48		0.27	
P	1498	4	1381	7	<141.15		485	13	2296	4		2153	7	1764	6	360	23	1121	7	1354	6	1123	
Sc	36	4	35	11	36	15	39	11	31	7	30.97	31	25	63	3	<36.47		60	10	68	6	61	10
V	283	3	202	5	273	5	212	5	354	4	252.2	163	7	172	5	141	10	213	5	176	5	182	21
Cr	302	5	364	23	205	38	<129.80		134	17		975	8	2418	6	1069	17	<62.66		<128.98		<221.14	8
Co											16.08	127	42	94	16	<247.27		<64.27		<47.18		<172.37	
Ni	164	26	<574.37		<773.91		<519.95		210	33		108	10	84	7	<11.22		127	8	92	8	98	
Cu	110	4	97	13	151	12	116	12	181	8		97	7	100	6	30	11	58	7	65	6	47	13
Rb	74	3	56	6	36	8	68	6	80	5	75.91	769	5	792	5	542	6	729	5	766	5	666	9
Sr	991	3	818	3	292	4	412	4	912	3	942.29	15	13	8	6	7	26	20	7	21	6	16	6
Y	17	4	15	9	10	12	13	10	18	8	16.35	37	11	31	6	17	19	51	7	56	6	46	15
Zr	40	4	32	10	13	15	16	13	41	7	31.97	1.70	20	1.56	9	0.81	35	0.83	16	1.29	12	0.67	11
Nb	0.92	9	0.58	35	0.35	46	0.43	42	1.14	22	1.53	279.90	7	301.14	6	136.61	10	171.72	7	196.82	7	132.88	43
Ba	213	4	158	7	73	11	94	9	247	5	256	3.25	15	3.23	8	<1.59		1.71	12	2.12	11	0.92	10
Cs	1.93	7	1.40	25	1.21	27	2.76	18	2.43	14	2	14.08	10	10.44	7	5.66	18	11.21	8	12.92	7	10.61	32
La	13.09	4	9.76	11	2.79	20	5.98	13	10.73	8	11.25	30.64	8	21.42	6	14.10	13	26.40	6	28.43	6	24.24	14
Ce	30.01	4	26.48	7	8.78	11	13.57	9	20.19	6	29.05	4.21	16	2.37	8	1.87	33	4.04	10	4.59	8	3.04	10
Pr	4.61	5	3.21	16	1.73	20	2.28	18	2.76	13	4.02	18.08	20	12.86	8	<6.53		18.70	11	23.47	8	18.81	25
Nd	22.12	5	15.35	18	7.24	28	9.32	22	14.94	13	17	7.68	29	2.59	15	1.28	206	3.58	30	4.70	17	<6.24	24
Sm	4.39	11	2.99	42	<9.94		3.64	36	6.35	22	5.06	1.58	43	0.94	14	<1.77		2.26	18	2.01	15	<1.79	
Eu	1.49	10	1.15	36	0.70	45	0.81	42	0.98	30	1.66	5.38	41	1.67	19	<4.40		4.63	25	5.63	15	<6.20	
Gd	3.82	12	3.21	46	2.78	41	2.90	40	5.47	24	4.69	0.80	38	0.23	21	<0.57		0.62	26	0.74	17	<0.63	
Tb	0.52	12	0.84	31	<0.33		<0.26		0.89	23	0.64	<0.64		0.26	18	0.23	62	0.79	21	1.00	14	<0.73	
Dy											2.89	2.67	31	0.68	20	<1.76		2.16	22	2.02	17	2.67	
Ho	0.72	11	0.12	74	0.43	53	0.47	44	0.62	29	0.79	<0.27		0.14	17	<0.39		0.28	25	0.28	18	<0.27	44
Er											1.6	<1.96		0.70	21	<3.52		1.96	24	2.20	18	1.83	
Tm											0.192	<0.31		0.09	22	<1.13		<0.05		0.07	37	<0.52	58
Yb	1.72	12	0.88	48	0.45	84	1.75	38	1.45	33	1.06	8.15	15	13.78	7	5.15	18	6.36	10	8.67	9	4.93	
Lu	0.19	15	0.21	54	0.14	40	0.12	47	0.21	35	0.356	2.44	19	3.47	8	0.66	42	2.25	11	2.41	10	1.60	24
Hf	1.09	16	1.47	42	<4.55		0.72	59	0.53	57	0.68	0.31	53	1.21	10	0.47	48	0.77	18	0.91	15	0.57	27
Ta	0.04	35	1.06	22	<1.42		<0.70		0.12	48	0.026	<152.01		27.72	19	<295.18		5.89	84	<13.64		25.22	42
Pb	10.91	5	7.99	17	7.41	18	7.19	17	17.74	7	12.27	6.31	46	4.75	15	4.64	38	5.88	25	5.95	20	<32.81	46
Th	2.52	7	2.60	19	0.73	34	2.56	19	2.18	15	3.12												
U	1.08	10	0.81	34	0.43	45	0.75	34	1.10	20	1.07												
B	40.56	15	19.26	64	<61.07		<295.82		11.03	93													
Li	8.87	12	<13.21		<16.15		<11.78		8.15	29													

All the analyses are completed in Zurich except 6 which is performed in Perugia.

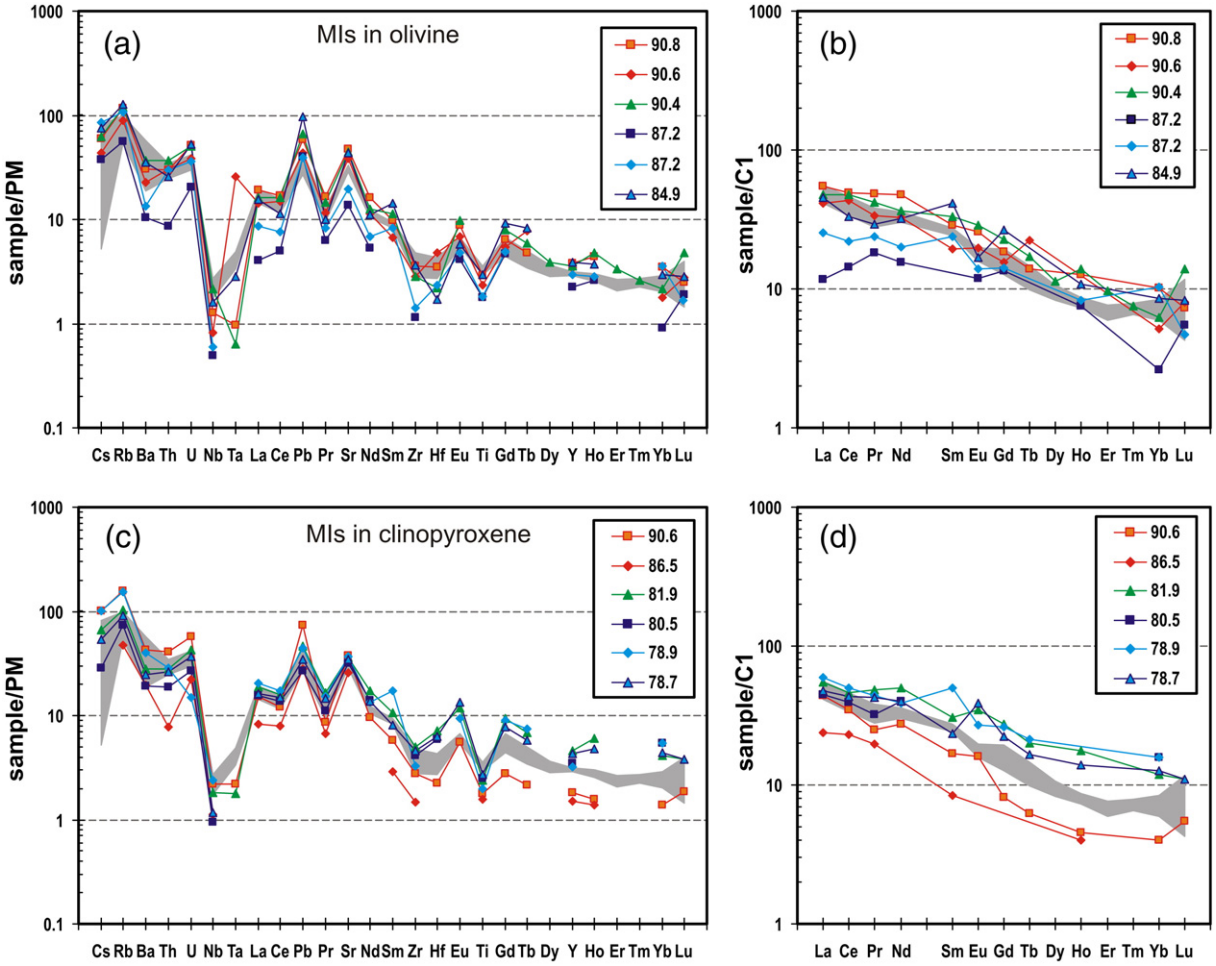

Fig. 9. (a, c) Primitive mantle-normalized trace element patterns and (b, d) chondrite-normalized REE patterns of melt inclusions (MIs) from olivine and clinopyroxene of SG12. Data source from Table 5. Shaded area shows the patterns of ankaramite whole rocks. Normalizing values from Sun and McDonough (1989). The very high Ta content in the melt inclusion Mg#90.6, most probably, is the result of spike in the LA signal. Digits in the legend mean the Mg # of the host mineral.

The oxygen fugacity of the magma was calculated using the method of Ballhaus et al. (1991). The method is strictly valid only for orthopyroxene-bearing assemblages, but its application to non-orthopyroxene rocks introduces only very small errors (<0.2 log units). Fugacities were calculated for each mineral pair at 0.7 GPa. The calculated values for the same core olivine–spinel pairs used for the geothermometry calculations cluster around ΔFMQ + 2.9. These values lie at the upper end of the oxygen fugacity range typical of arc lavas (ΔFMQ + 1 to ΔFMQ + 3; Ballhaus et al., 1991; Eggins, 1993). The estimates for rim olivine–spinel pairs are slightly higher (ΔFMQ + 3.6) reflecting increasing oxidation during crystallization.

8. Diffusion of Fe and Ca from the melt inclusions into olivine

The low MgO and FeO contents of the unheated melt inclusions analyzed by electron microprobe compared to their bulk composition determined by LA-ICPMS (Table 4) reflect considerable post-entrapment growth of olivine on the wall of the melt inclusions and potential diffusion of FeO into the host mineral. These processes have been described in details by Danyushevsky et al. (2000, 2002), who demonstrated that the degree of modification of the melt inclusions strongly depend on the cooling rate and chemical composition of the melt and host. The submarine emplacement and glassy nature of the groundmass of the cumulate SG12 suggest that the entire chemical modification of the melt inclusions most probably occurred before the eruption of the lava. Considering the crystallization temperature difference between the core and the rim of the olivine, we can obtain the cooling interval at which the modification of the chemistry of the melt inclusions occurred. Our calculation from Table 6 shows that the re-equilibration occurred in a temperature interval of ~100–120 °C, suggesting a comparatively long-lasting process of crystallization and cooling in the magma chamber, which is consistent with the cumulitic nature of this rock.

In order to understand the behaviour of FeO, MgO and CaO during the cooling, we performed high-resolution (2 to 3 μm steps) profiles around the two melt inclusions, shown in Fig. 8e and d, entrained in the core and rim, respectively. The inclusions are located near the spinel–olivine pairs that have already been used for the calculation of temperature. The results for the FeO and CaO contents of the profiles are shown in Fig. 10. The chemical zonation around the inclusions is reflected into a thin zone of high-Fe olivine, which can be seen in Fig. 8f. The decrease of FeO from ~10 to 9.4 wt.% and CaO from 0.52 to 0.43 wt.% around the larger (42 μm) melt inclusion hosted in olivine ($Fo_{90.4–90.8}$) occurs within ~15 μm from the boundary of the inclusion. The profile around the smaller (20 μm) melt inclusion in the olivine rim ($Fo_{84.9–85.1}$) exhibits a decrease of FeO from ~16.5 to 14.2 wt.% and CaO from 0.63 to 0.42 wt.% within a zone <10 μm, which seems to reflect a shorter cooling interval. The two profiles undoubtedly demonstrate decrease of CaO and FeO from the rim of melt inclusions towards the host olivine. Similar CaO-profiles around high-Ca melt inclusions in olivines from South Sulawesi (Elburg et al., 2006) have been interpreted as the result of post-entrapment equilibration between olivine and high-Ca ankaramitic melt. We favour a similar hypothesis for the melt inclusions in the cumulate SG12.

9. Discussion

9.1. Relationships between the cumulate, high-K ankaramites and associated mafic shoshonites

Shoshonitic magmas are widespread in continental arc settings such as the Aeolian Volcanic Arc (Francalanci et al., 2007), the Eastern Rhodopes, Bulgaria (Marchev et al., 2004), the Tibetan Plateau (Turner et al., 1996), the Mexican Volcanic Belt (Blatter et al., 2001) and, more rarely, in back-arc settings or oceanic island arcs (e.g. Izu–Bonin–Mariana arc; Sun and Stern, 2001). The most primitive compositions in many of these high-K series are rare absarokites with comparatively high Mg# and Ni and Cr contents, which are believed to represent the parental magma for the more evolved compositions (e.g. Hesse and Grove, 2003). The occurrence of more mafic high-K ankaramitic melt inclusions and lavas within high-Fo olivines (up to Fo_{91}) in the Srednogorie zone, Aeolian Islands (Gioncada et al., 1998) and South Sulawesi (Elburg et al., 2006) suggest, however, that nepheline-normative potassic ankaramites are a more likely parental magma type for the more evolved members of the shoshonitic series.

The most mafic rocks from the Yambol–Burgas region show isotope evidence for very limited interaction with the crust (Georgiev, 2008). Therefore, the influence of this process will have comparatively small impact on their major and trace element budget. This is confirmed by the similarity of major and trace element composition between the ankaramitic lavas and the olivine- and clinopyroxene-hosted melt inclusions in the cumulate rock SG12 (Fig. 9). Many lines of evidence suggest that the cumulates, ankaramites and more evolved rocks are genetically related and that accumulation and fractional crystallization played a major role in their evolution. These include (1) the similarity of the major and trace element compositions of the clinopyroxenes in the cumulates, ankaramites and shoshonites, along with the similarity between spinels from the cumulates and absarokites; (2) the occurrence of rare very high-Mg clinopyroxenes in the shoshonitic basalts, which can be interpreted as a direct petrographic evidence for the genetic relationship with the less evolved magmas; and (3) the increase of alkalis and Al_2O_3, LILE and HFSE and decrease of CaO, FeO and MgO at very small increase of SiO_2 from ankaramites to shoshonitic basalts. Petrographic observations indicate that the aforementioned geochemical features can be explained by accumulation and fractionation of a clinopyroxene–olivine-dominated assemblage.

The capability of ankaramite to produce shoshonitic basalt involving clinopyroxene and olivine fractionation was quantitatively tested using a least-squares major element mass-balance calculation with the program PetroGraph of Petrelli et al. (2005). As input data, we used averaged major element composition of the minerals from Tables 2 and 3 in the Appendix. Our model (Table 7) is largely able to reproduce the evolution of the ankaramite magma towards the more evolved members. The most consistent model was obtained for the transition from the ankaramitic melt hosted in the high-Fo olivine to the absarokite-like composition of the melt in the low-Fo olivine rim of sample SG12. The transition can be explained by combined olivine–clinopyroxene fractionation at a ratio >1:3. Conversely, accumulation of the two minerals is able to produce cumulitic rocks like SG12. Our model further suggests that fractionation of olivine and clinopyroxene at higher ratios (1:4 to 1:6) is able to produce shoshonite-like high-Al basalts from absarokites. These calculations, however, have relatively high squares of residuals. The most reasonable explanation for this discrepancy is either the more complicated character of the fractionation–accumulation process or the difficulties in the selection of proper chemical compositions for the fractionated minerals. All in all, the results of the modelling are in agreement with the petrographic observations and indicate that they can explain the geochemical variations.

Table 6
Temperature, pressure and fO_2 estimation for cumulitic rock SG12 and ankaramites (SG090 and SG097).

Sample *N*/method	SG12	SG090	SG097
Estimated magmatic temperatures (°C)			
ol–sp, Ballhaus et al. (1991, 1994)	Core-1093-1124; Ol Fo90.6-90.0, Sp Cr#0.48		
ol–sp, Ballhaus et al. (1991, 1994)	Rim 1018; Ol (Fo85.1), Sp Cr#0.698		
ol–liquid, Putirka (1997)	1214–1240		
ol–liquid, Beattie (1993)	1218–1321		
ol–liquid, Langmuir et al. (1992)	1146–1198		
ol–cpx, Loucks (1996)	1217–1256		
cpx–sat, Putirka et al. (2003)	1173–1214	1230–1259	1182–1194
cpx–liquid Putirka et al. (2003)	1266–1290	1304–1363	1252–1271
cpx–liquid Model 1 Putirka et al. (1996)	1252–1241	1245–1311	1214–1242
cpx–liquid Model 2 Putirka et al. (1996)	1218–1243	1238–1290	1207–1230
Estimated pressures (GPa)			
cpx–liquid, Putirka et al. (2003)	0.67–0.82	0.74–1.23	0.52–0.74
cpx–liquid, Model 1 Putirka et al. (1996)	0.75–0.93	0.73–1.42	0.61–0.93
cpx–liquid, Model 2, Putirka et al. (1996)	0.71–0.86	0.70–1.33	0.59–0.88
Estimated magmatic fO_2 (Δ log FMQ)			
ol–sp, Ballhaus et al. (1991, 1994)	Core 2.84 at 0.6 Gpa Ol (Fo90.0), Sp (Cr# 0.747)		
ol–sp, Ballhaus et al. (1991, 1994)	Core 2.96 at 0.6 Gpa Ol (Fo90.6), Sp (Cr# 0.747)		
ol–sp, Ballhaus et al. (1991, 1994)	Rim 3.64 at 0.6 Gpa Ol (Fo85.1), Sp (Cr#0.698)		

9.2. Does the ankaramite magma represent a liquid composition?

The high amount of clinopyroxene phenocrysts, which is a typical petrographic feature of the ankaramites all over the world, led many authors to reject the existence of primitive high-CaO and CaO/Al_2O_3 ankaramitic magmas (e.g. Gunn et al., 1970; Hughes, 1982).

The results of our current study, however, showed that the major and trace element compositions of the ankaramites are similar to those of the melt inclusions hosted in high-Mg olivine and clinopyroxene from the cumulitic rock from the same region. In addition, the high-Ca nature of these melts is confirmed by the CaO content of the olivine (0.53 to 0.40 wt.%), which is much higher than the typical values in most subduction-related magmas (0.25–0.15 wt.%). The decrease of CaO from melt inclusion into the host olivine crystals in the high-resolution microprobe profiles further confirms that the high-Ca content of the melt inclusions is a primary feature of the ankaramitic magma. Therefore, although effects of crystal accumulation cannot be entirely excluded, the whole rock compositions of the ankaramite lavas nearly reflect the liquid compositions.

9.3. Origin of the ankaramites

Ultra-calcic melt inclusions and lavas (CaO/Al_2O_3 weight ratio >1.1) have been identified in a number of geological environments (see Schiano et al., 2000 for a review). Based on their composition, ultra-calcic melts have been divided into two groups (Schiano et al., 2000; Kogiso and Hirschmann, 2001): a silca-poor, hypersthene-normative group; and an alkali-rich, nepheline-normative group. The first group is found in mid-ocean ridges, back-arcs, and ocean islands, whereas the second group is typical of arc environments. Ultra-calcic melts from the Eastern Srednogorie are typical representatives of the second group and more specifically of a subgroup of high-K (shoshonitic) ankaramites, which have been identified so far in the Aeolian islands of

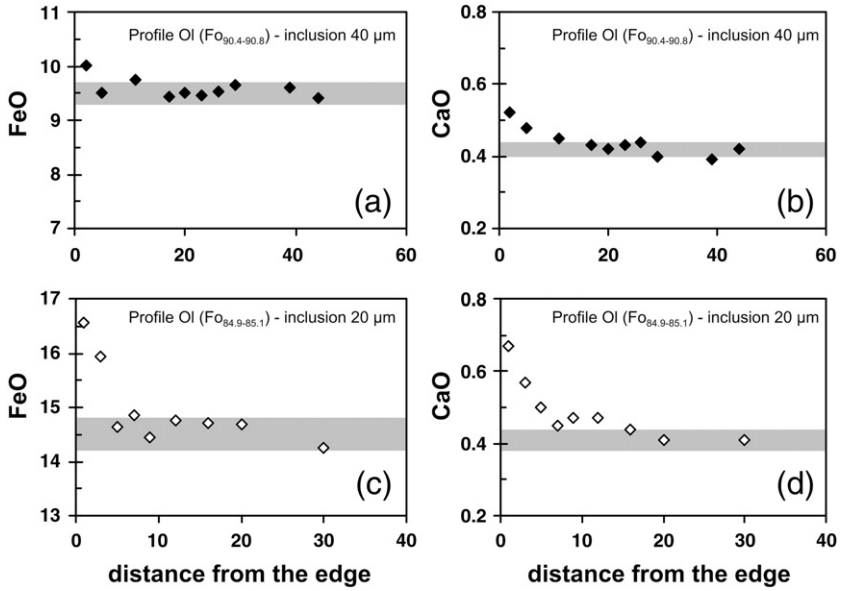

Fig. 10. FeO and CaO (wt.%) profiles in olivine phenocrysts around two melt inclusions from sample SG12. The inclusions and location of the profiles can be seen in Fig. 8d, e.

Volcano and Stromboli (Metrich and Clocchiati, 1996; Gioncada et al., 1998) and the West Sulawesi Volcanic Province, Indonesia (Elburg et al., 2006).

The two groups of unusually Ca-enriched (ankaramitic) magmas likely originate from different sources. Hypersthene-normative ultracalcic lavas have been experimentally obtained by low-degree melting of a refractory lherzolite or harzburgite mantle, depleted by previous melting event(s) (Schmidt et al., 2004; Green et al., 2004; Kogiso and Hirschmann, 2001). Although initially obtained melts are not very calcic, they have typically ankaramitic CaO/Al_2O_3 ratios. Fractionation of olivine may increase their CaO to higher values. Higher Na_2O and K_2O in the melts could be achieved by addition of $CO_2 + H_2O$ fluid from a subducting slab (Schmidt et al., 2004) or dolomitic carbonatite melt formed in the wedge (Green et al., 2004). A major problem at which these models have to face is the high temperature (>1350 °C) required for the melting of the refractory sources, which even with addition of volatiles will be decreased by only 20–30 °C.

Nepheline-normative Ca-rich melts, however, cannot be produced by partial melting of common lherzolite mantle compositions. Generation of such magmas has been predicted through thermodynamic calculations and trace element modelling of intermediate to high degree partial melting of lower crustal or upper mantle pyroxenites (Schiano et al., 2000). Recently, such melts have been successfully obtained in melting experiments with variable Ca-rich pyroxene + olivine + amphibole assemblages at 0.5–1 GPa and temperatures of 1175–1350 °C (Médard et al., 2004, 2006). Such assemblages are observed as parts of exposed old arc ultramafic/mafic cumulate complexes in the Talkeetna area, Alaska (DeBari and Coleman, 1989; DeBari and Sleep, 1991; Kelemen et al., 2003), the Kohistan Terrane of North Pakistan (Khan et al., 1993; Miller and Christensen, 1994; Burg et al., 1998; Ringuette et al., 1999; Jagoutz et al., 2007), and the Ivrea Zone in North Italy (Mehnert, 1975; Rivalenti et al., 1984; Quick et al., 1994). These complexes have been interpreted to be remnants of magma chambers emplaced at the base of the crust, close to the upper mantle–lower crust transition. Cumulitic xenoliths, forming series of ultramafic–mafic to gabbroic rocks, have been found in many calc-alkaline magmas of active arcs (e.g. Aleutian arc, Conrad and Kay, 1984) or in intraplate basalts (e. g. Penghu Islands, South China Sea, Ho et al., 2000; Lake Balaton and Nógrád-Gömör Volcanic field, Pannonian Basin, Hungary, Dobosi et al., 2003; Kovács et al., 2004; Zajacz et al., 2007). Marchev et al. (2006) describe a series of xenoliths, including clinopyroxene–amphibole varieties, entrained in alkaline basalts from the Rhodope Massif. They were interpreted to indicate a large event of underplating of alkaline basaltic magma at the crust–mantle boundary, prior to intraplate basaltic and orogenic Lower Oligocene volcanism. Therefore, it seems like that these cumulitic lithologies are a suitable source for the model of Médard et al. (2006).

Application of this model for the generation of the Yambol–Burgas ankaramites has been explored by Georgiev (2008). The author used clinopyroxene and amphibole–clinopyroxene cumulates entrained in a basaltic dyke from Yambol–Burgas region as a model source. Calculation of the possible partial melts confirms the conclusions that the CaO/Al_2O_3 ratio of melt is controlled mostly by the abundance of clinopyroxene in the source. The modelled liquid matches reasonably well the compositions of most elements in the ankaramites and melt inclusions except for slightly lower K, Rb, MREE, U, Th and Sr. However, the simple amphibole–clinopyroxene cumulate melting model contradicts with the radiogenic isotope data for the cumulates and ankaramites. Cumulitic pyroxenites from the Eastern Srednogorie have slightly less radiogenic Sr isotopes and much lower $^{206}Pb/^{204}Pb$ and $^{208}Pb/^{204}Pb$ isotope ratios compared to the cumulate SG12 and the ankaramitic lavas. To explain these discrepancies, Georgiev (2008) offered a more complicated model involving higher K_2O contents in the wehrlite source (by phlogopite or fluids), along with chemical and thermal interaction, at the crust–mantle boundary, with (i) spinel–peridotite-derived melts having subduction-modified trace element and isotopic signature, and (ii) more radiogenic crustal lithologies.

Some of the problems with the application of the cumulate-remelting model have been discussed by Elburg et al. (2007). One of them, the relatively low Mg/Fe ratios of the melt and the low-Fo content of the olivines in the experiments (Fo<89) compared to the natural observations, is valid also for the Eastern Srednogorie ankaramitic

Table 7
Least squares major element mass-balance models of fractional crystallization for different steps within the mafic rocks.

Parent	Daughter	ol	cpx	*F*	$\sum R^2$
jn27a15 (MI in Fo90)	au28a05 (MI in Fo85)	3.4	11.3	0.853	0.219
SG090 (ank)	SG102a (abs)	2.7	16.9	0.804	8.949
SG102a (abs)	Sg106 HAB	6.2	24.8	0.690	7.371
SG095 (abs)	Sg106 HAB	3.8	15.7	0.805	5.041

F — fraction of melt remaining in each fractionation step, $\sum R^2$ — sum of the squares of residuals, ol — olivine, cpx — clinopyroxene.

magmas. For the most Mg-rich olivines (Fo ~ 89), cumulitic experiments require temperatures of 1350 °C, which was reflected also in the melt with highest CaO/Al_2O_3 ratios, but with very low K_2O content. Although minor presence of phlogopite in the melting assemblage, can increase the K_2O/Na_2O ratio in the resulting melt, the high percentage of melting would reduce the final K_2O content. An additional discrepancy between the Eastern Srednogorie melt and the experimental study is the higher TiO_2 content in the latter (1.5–2.1 wt.%). These values are more typical for within-plate basalts, rather than for orogenic primitive melts.

Another important issue is the heat source for melting of the cumulates. Schiano et al. (2000) suggested that it could be either arc magmas passing through the lower crust or hot adiabatically upwelling mantle that produces water-poor arc magmas and heats the overlying crust. Petrographic observation on the Rhodope cumulitic rocks, entrained within the alkaline basalts, showed that the source cumulate bodies were not affected by the general increase of the temperature in the region, caused by asthenosphere upwelling (Marchev et al., 2004). Moreover, they survived even the high temperature influence of the host alkaline basalts, suffering only limited metasomatic exchange. Our petrographic observations on the entrained cumulitic rocks in the Srednogorie basalts also do not show petrographic evidence for melting.

Considering the nepheline-normative ankaramitic melts from Lombok, Elburg et al. (2007) suggested that they were generated from a metasomatised non-garnet mantle source, consisting of clinopyroxene and olivine, accompanied by either amphibole or jadeijtic clinopyroxene. On the bases of relatively flat whole rock HREE distribution of the high-K ankaramites of the Eastern Srednogorie, Georgiev (2008) also exclude the involvement of garnet in the melting process. Although HREE fractionation (Tb_n/Yb_n ratio > 1.5) of the melt inclusions, seems to require the presence of garnet in the source, we prefer to rely on the more precise whole rock HREE analyses which exclude garnet as a residual phase. Following Elburg et al. (2007), we suggest that Eastern Srednogorie nepheline-normative ankaramites originated from a garnet-free olivine–clinopyroxene mantle source. The high-K composition of the rocks, however, seems to require phlogopite, rather than amphibole or jadeijtic clinopyroxene. All in all, we conclude that the source of high-K ankaramites is either a lower crustal clinopyroxenite cumulate or a clinopyroxene- and phlogopite-enriched mantle portion. Interaction of a melt derived from a phlogopite-bearing mantle portion with overlying lower crustal clinopyroxenite cumulates cannot be excluded, and may be an effective way of producing the described ankaramites. However, complete justification of either theory requires further research.

10. Conclusions

In the Yambol–Burgas region of the Eastern Srednogorie arc the most mafic rocks are high-K (shoshonitic) nepheline-normative ankaramites. These rocks have geochemical characteristics consistent with primary magma compositions, e.g. Mg # of 73–61, Ni ~ 100 ppm and Cr > 400 ppm. The trace element composition of these rocks is typical of arc magmas, very similar to other well-known continental and oceanic island arcs such as the Aeolian arc, Tibet, and South Sulawesi.

Major and trace element compositions of olivine- and clinopyroxene-hosted melt inclusions in a cumulitic rock, formed by accumulation of olivine and clinopyroxene phenocrysts from ankaramitic lava, provide us with unequivocal evidence for the existence of primary high-K ankaramitic magmas in the Eastern Srednogorie continental arc. The parental ankaramitic magma was silica undersaturated with high-CaO (>12 wt.%), CaO/Al_2O_3 ratio >1 and ~10–11 wt.% MgO. The deficiency of total oxide contents in the melt inclusions suggest that the melt contained ~3 wt.% H_2O, which is confirmed by the high $SiO_2/(MgO + FeO)$ ratios.

Although a range of chemical characteristics of the ankaramites can be produced by partial melting of clinopyroxenite cumulitic rocks in the crust, the discrepancy in the radiogenic isotope ratios between the ankaramites and the cumulates, along with high-Fo composition of olivine in the ankaramites, make this scenario hardly likely. Interaction of mantle-derived magmas with such a material, however, is able to increase the Ca content of the mantle-derived melt. In accordance with the flattened HREE patterns in the ankaramite whole rocks and high-K content of the Yambol–Burgas region, we suggest a garnet-free clinopyroxene- and phlogopite-bearing mantle source.

The chemical variations from the high-K ankaramites through the absarokites and shoshonitic basalts indicate that they were co-magmatic and were produced by fractionation of olivine and clinopyroxene.

Acknowledgments

This study was carried out cooperatively between the Bulgarian Academy of Sciences (Geological Institute), ETH, Zürich (Department of Earth Sciences), and Consiglio Nazionale della Richerche (University of Florence). Microprobe analyses were done with the assistance of O. Vaselli, K. Petrone and C. Ginibre. We are grateful to F. Caponi for the XRF analyses. Constructive comments from P. Leat, S. Arai and an anonymous reviewer helped to clarify our ideas. Editorial suggestions of Andrew Kerr are appreciated. We thank Yildirim Dilek for his editorial efforts in organizing this volume.

Appendix A. Supplementary data

Supplementary data associated with this article can be found, in the online version, at doi:10.1016/j.lithos.2009.03.014.

References

Aiello, E., Bartolini, C., Boccaletti, M., Gocev, P., Karagjuleva, J., Kostadinov, V., Manetti, P., 1977. Sedimentary features of Srednogorie Zone (Bulgaria) — Upper Cretaceous intra-arc basin. Sedimentary Geology 19, 39–68.

Antonijevic, I., Grubic, A., Djordjevic, M., 1974. The Upper Cretaceous paleorift in Eastern Serbia. In: Karamata, S. (Ed.), Metallogeny and Concepts of the Geotectonic Development of Yugoslavia, pp. 315–339.

Arai, S., 1994. Compositional variation of olivine–chromite in Mg-rich magmas as a guide to their residual spinel peridotites. Journal of Volcanology and Geothermal Research 59, 279–293.

Ballhaus, C.G., Berry, R.F., Green, D.H., 1991. High pressure calibration of the olivine–orthopyroxene–spinel oxygen barometer, implications for the oxidation sate of the upper mantle. Contributions to Mineralogy and Petrology 107, 7–40.

Ballhaus, C., Berry, R.F., Green, D.H., 1994. High pressure experimental calibration of the olivine–orthopyroxene–spinel oxygen geobarometer: implications for the oxidation state of the upper mantle—Erratum. Contribution to Mineralogy and Petrology 118, 109.

Barsdell, M., Berry, R.F., 1990. Origin and evolution of primitive island arc ankaramites from Western Epi, Vanuatu. Journal of Petrology 31, 747–777.

Beattie, P., 1993. Olivine–melt and orthopyroxene–melt equilibria. Contributions to Mineralogy and Petrology 115, 103–111.

Blatter, D.L., Carmichael, I.S.E., Deino, A., Renne, P.R., 2001. Neogene volcanism at the front of the central Mexican volcanic belt: basaltic andesites to dacites, with contemporaneous shoshonites and high-TiO_2 lava. Geological Society of America Bulletin 113, 1324–1342.

Boccaletti, M., Manetti, P., Peccerillo, A., 1974. Hypothesis on plate tectonic evolution of Carpatho-Balkan Arcs. Earth and Planetary Science Letters 23, 193–198.

Boccaletti, M., Manetti, P., Peccerillo, A., Stanisheva-Vassileva, G., 1978. Late Cretaceous high-potassium volcanism in Eastern Srednogories, Bulgaria. Geological Society of America Bulletin 89, 439–447.

Burg, J.P., Bodinier, J.L., Chaudhry, S., Hussain, S., Dawood, H., 1998. Infra-arc mantle–crust transition and intra-arc mantle diapirs in the Kohistan complex (Pakistani Himalaya): petro-structural evidence. Terra Nova 10, 74–80.

Cheshitev, G., Kanchev, I. (Eds.), 1989. Geological Map of P. R. Bulgaria, 1:500 000. Sofia. Bulgaria. Supreme Technical Council.

Ciobanu, C.L., Cook, N.J., Stein, H., 2002. Regional setting and geochronology of the Late Cretaceous Banatitic Magmatic and Metallogenetic Belt. Mineralium Deposita 37, 541–567.

Conrad, W.K., Kay, R.W., 1984. Ultramafic and mafic inclusions from Adak Island: crystallization history and implications for the nature of primary magmas and crustal evolution in the Aleutian island arc. Journal of Petrology 25, 88–125.

Csontos, L., 1995. Tertiary tectonic evolution of the Intra-Carpathian area: a review. Acta Volcanologica 7, 1–13.

Dabovski, C., Harkovska, A., Kamenov, B., Mavroudchiev, B., Stanisheva-Vassileva, G., Yanev, Y., 1991. A geodynamic model of the Alpine magmatism in Bulgaria. Geologica Balcanica 21, 3–15.

Dabovski, C., Kamenov, B., Vassilev, E., in press. Upper Cretaceous Geology. Magmatism. In: Zagorchev, I., Dabovski, C., Nikolov, T. (Eds.), Geology of Bulgaria. Volume II. Mesozoic geology. Sofia, Academic Publishing House "Prof. Marin Drinov", 423-553 (in Bulgarian).

Daieva, L., Stanisheva-Vassileva, G., 2002. Sediment involvement in the genesis of subduction-related volcanic rocks from Eastern Srednogorie island arc system: trace element data. Geologica Balcanica 32 (2–4), 33–36.

Danyushevsky, L.V., Della-Pasqua, F.N., Sokolov, S., 2000. Reequilibration of melt inclusions trapped by magnesian olivine phenocrysts from subduction-related magmas: petrological implications. Contributions to Mineralogy and Petrology 138, 68–83.

Danyushevsky, L.V., Sokolov, S., Falloon, T.J., 2002. Melt inclusions in olivine phenocrysts: using diffusive re-equilibration to determine the cooling history of a crystal, with implications for the origin of olivine–phyric volcanic rocks. Journal of Petrology 43, 1651–1671.

Danyushevsky, L.V., Leslie, R.A.J., Crawford, A.J., Durance, P., 2004. Melt inclusions in primitive olivine phenocrysts: the role of localized reaction processes in the origin of anomalous compositions. Journal of Petrology 45, 2531–2553.

DeBari, S.M., Coleman, R.G., 1989. Examination of the deep levels of an island arc: evidence from the Tonsina ultramafic–mafic assemblage, Tonsina, Alaska. Journal of Geophysical Research 94, 4373–4391.

DeBari, S.M., Sleep, N.H., 1991. High-Mg, low-Al bulk composition of the Talkeetna island arc, Alaska: implications for primary magmas and the nature of arc crust. Geological Society of America Bulletin 103, 37–47.

Della-Pasqua, F.N., Varne, R., 1997. Primitive ankaramitic magmas in volcanic arcs: a melt inclusion approach. Canadian Mineralogyst 35, 291–312.

Dewey, J., Pitman, W., Ryan, W., Bonnin, J., 1973. Plate tectonics and evolution of the Alpine system. Geological Society of America Bulletin 84, 3137–3180.

Dobosi, G., Downes, H., Embey-Isztin, A., Jenner, G.A., 2003. Origin of megacrysts and pyroxenite xenoliths from the Pliocene alkali basalts of the Pannonian Basin (Hungary). Neues Jahrbuch Abhandlungen 178 (3), 217–237.

Eggins, S.M., 1993. Origins and differentiation of picritic arc magmas, Ambae (Aoba), Vanuatu. Contributions to Mineralogy and Petrology 114, 79–100.

Elburg, M.A., Kamenetski, V.S., Nikogosian, I., Foden, J., Sobolev, V., 2006. Coexisting high- and low-calcium melts identified by mineral and melt inclusion studies of a subduction–influenced syncollisional magma from south Sulawesi, Indonesia. Journal of Petrology 47, 2433–2462.

Elburg, M.A., Kamenetski, V.S., Foden, J., Sobolev, V., 2007. The origin of medium-K ankaramitic arc magmas from Lombok (Sunda arc, Indonesia): mineral and melt inclusion evidence. Chemical Geology 240, 260–279.

Falloon, T.J., Danyushevsky, L.V., 2000. Melting of refractory mantle at 1.5, 2 and 2.5 GPa under anhydrous and H_2O-undersaturated conditions: implications for the petrogenesis of High-Ca boninites and the influence of subduction components on mantle melting. Journal of Petrology 41, 257–283.

Francalanci, L., Avanzinelli, R., Tommasini, S., Neuman, A., 2007. A west–east geochemical and isotopic traverse along the volcanism of the Aeolian Island arc, southern Tyrrhenian Sea, Italy: inferences on mantle source processes. Geological Society of America Special Paper 418, 236–263.

Fügenschuh, B., Schmid, S.M., 2005. Age and significance of core complex formation in a very curved orogen: evidence from fission track studies in the South Carpathians (Romania). Tectonophysics 404, 33–53.

Gaetani, G.A., Grove, T.L., 1998. The influence of water on melting of mantle peridotite. Contributions to Mineralogy and Petrology 131, 323–346.

Gaetani, G.A., Cherniak, D.J., Watson, E.B., 2002. Diffusive reequilibration of CaO in olivine-hosted melt inclusions. Geochimica and Cosmochimica Acta 66 (15A), A254.

Georgiev, S., 2008. Sources and evolution of Late Cretaceous magmatism in Eastern Srednogorie, Bulgaria: constraints from petrology, isotope geochemistry and geochronology. PhD thesis, ETH Zurich.

Georgiev, G., Dabovski, C., Stanisheva-Vassileva, G., 2001. East Srednogorie-Balkan rift zone. In: Ziegler, P.A., Cavazza, W., Robertson, A.H.F., Crasquin-Soleau, S. (Eds.), Peri-Tethys Memoir 6: Peri-Tethyan Rift/Wrench Basins and Passive Margins. Mémoirs du muséum national d'histoire natural, vol. 186. Paris, pp. 259–293.

Gioncada, A., Clocchiatti, R., Sbrana, A., Bottazzi, P., Massare, D., Ottolini, L., 1998. A study of melt inclusions at Vulcano (Aeolian Islands, Italy): insights on the primitive magmas and on the volcanic feeding system. Bulletin of Volcanology 60, 286–306.

Green, D.H., Schmidt, M.W., Hibberson, W.O., 2004. Island-arc ankaramites: primitive melts from fluxed refractory lherzolitic mantle. Journal of Petrology 45, 391–403.

Gunn, B.M., Coy-Yll, R., Watkins, N.D., Abranson, C.E., Nougier, J., 1970. Geochemistry of an oceanite–ankaramite–basalt suite from East Island, Crozet Archipelago. Contributions to Mineralogy and Petrology 28, 319–339.

Halter, W.E., Pettke, T., Heinrich, C.A., Rothen-Rutishauser, B., 2002. Major and trace element analyses of melt inclusions by laser-ablation ICP-MS: methods of quantification. Chemical Geology 183, 63–86.

Hesse, M., Grove, T.L., 2003. Absarokites from the western Mexican volcanic belt: constraints on mantle wedge conditions. Contributions to Mineralogy and Petrology 146, 10–27.

Hirschmann, M., Wiens, D., Peacock, S., 2000. Subduction Factory Science Plan: NSF Margins Initiative. http://www.ldeo columbia.edu/margins/SF_Sci_Plan_revised.pdf, 42 p.

Ho, K.S., Chen, J.C., Alan, D.S., Juang, W.S., 2000. Petrogenesis of two groups of pyroxenite from Tungchihsu, Penghu Islands, Taiwan Strait: implications for mantle metasomatism beneath SE China. Chemical Geology 167, 355–372.

Hsu, K., Nachev, I., Vuchev, V., 1977. Geologic evolution of Bulgaria in the light of plate tectonics. Tectonophysics 40, 245–256.

Hughes, C.J., 1982. Igneous Petrology. Elsevier, Amsterdam, The Netherlands.

Ivanov, R., 1979. To the tectonogeochemical analysis of the Upper Cretaceous magmatism in the East Srednogorie. Review of the Bulgarian Geological Society 40 (1), 47–61 (in Bulgarian with English abstract).

Jagoutz, O., Müntener, O., Ulmer, P., Pettke, T., Burg, J.-P., Dawood, H., Hussain, S., 2007. Petrology and mineral chemistry of lower crustal intrusions: the Chialas Complex, Kohistan (NW Pakistan). Journal of Petrology 48, 1895–1953.

Jankovic, S., 1997. The Carpatho-Balkanides and adjacent area: a sector of the Tethyan Eurasian metallogenic belt. Mineralium Deposita 32, 426–433.

Jurewicz, A.J.G., Watson, E.B., 1988. Cations in olivine. Calcium partitioning and calcium–magnesium distribution between and olivines and coexisting melts, with petrologic applications. Contributions to Mineralogy and Petrology 99, 176–185.

Kamenetsky, V.S., Crawford, A.J., Meffre, S., 2001. Factors controlling chemistry of magmatic spinel: an empirical study of associated olivine, Cr-spinel and melt inclusions from primitive rocks. Journal of Petrology 42, 655–671.

Kelemen, P.B., Hanghøj, K., and Green, A.R., 2003. One view of the Geochemistry of subduction-related magmatic arcs, with an emphasis on Primitive andesite and lower crust, pp. 593–659. In: The Crust (ed. Rudnick, R. L.) vol. 3, Treatise on Geochemistry (eds. H.D. Holland and K.K. Turekian), Elsevier-Pergamon, Oxford.

Khan, M.A., Jan, M.Q., Weaver, B.L., 1993. Evolution of the lower arc crust in Kohistan, N. Pakistan: temporal arc magmatism through early, mature and intra-arc rift stages. Geological Society London Special Publication 74, 123–138.

Kennedy, A.K., Hart, S.R., Frey, F.A., 1990. Composition and isotopic constraints on the petrogenesis of alkaline arc lavas. Lihir Island, Papua New Guinea. Journal of Geophysical Research 95, 6929–6942.

Kogiso, T., Hirschmann, M.M., 2001. Experimental study of clinopyroxenite partial melting and the origin of ultra-calcic melt inclusions. Contributions to Mineralogy and Petrology 142, 347–360.

Kovács, I., Zajacz, Z., Szabó, C., 2004. Type-II xenoliths and related metasomatism from the Nógrád-Gömör Volcanic Field, Carpathian–Pannonian region (northern Hungary–southern Slovakia). Tectonophysics 393, 139–161.

Kress, V.C., Carmichael, I.S.E., 1991. The compressibility of silicate liquids containing Fe_2O_3 and the effect of composition, temperature, oxygen fugacity and pressure on their redox states. Contributions to Mineralogy and Petrology 108, 82–92.

Langmuir, C.H., Klein, E.M., Plank, T., 1992. Petrological systematics of mid-ocean ridge basalts: Constraints on melt generation beneath ocean ridges. In: Morgan, J.P., Blackman, D.K., Sinton, J.M. (Eds.), Mantle Flow and Melt Generation at Mid-ocean Ridges, pp. 183–280.

Leat, P.T., Riley, T.R., Wareham, C.D., Millar, I.L., Kelley, S.P., Storey, B.C., 2002. Tectonic setting of primitive magmas in volcanic arcs: an example from the Antarctic Peninsula. Journal of Geological Society of London 159, 31–44.

Lee, J., Stern, R.J., 1998. Glass inclusions in Mariana arc phenocrysts; a new perspective on magmatic evolution in a typical intra-oceanic arc. Journal of Geology 106, 19–33.

Le Maitre, R.W., Streckeisen, A., Zanettin, B., Le Bas, M.J., Bonin, B., Bateman, P., Bellieni, G., Dudek, A., Efremova, S., Keller, J., Lamere, J., Sabine, P.A., Schmid, R., Sorensen, H., Woolley, A.R., 2002. Igneous Rocks: a Classification and Glossary of Terms, Recommendations of the International Union of Geological Sciences, Subcommission of the Systematics of Igneous Rocks. Cambridge.

Libourel, G., 1999. Systematics of calcium partitioning between olivine and silicate melt: implication for melt structure and calcium content of magmatic olivine. Contributions to Mineralogy and Petrology 136, 63–80.

Loucks, R.R., 1996. A precise olivine–augite Mg–Fe-exchange geothermometer. Contributions to Mineralogy and Petrology 125, 140–150.

Manetti, P., Peccerillo, A., Poli, G., 1979. REE distribution in Upper Cretaceous calc-alkaline and shoshonitic volcanic rocks from Eastern Srednogorie (Bulgaria). Chemical Geology 26, 51–63.

Marchev, P., Raicheva, R., Downes, H., Vaselli, O., Chiaradia, M., Moritz, R., 2004. Compositional diversity of Eocene–Oligocene basaltic magmatism in the Eastern Rhodopes, SE Bulgaria: implications for genesis and tectonic setting. Tectonophysics 393, 301–328.

Marchev, P., Arai, S., Vaselli, O., 2006. Cumulate xenoliths series in the Krumovgrad alkaline basaltic and lamprophyric dykes: evidence for the existence of layered plutons under the Eastern Rhodope metamorphic core-complexes, Bulgaria. In: Dilek, Y., Pavlides, S. (Eds.), Post-collisional Tectonics and Magmatism in the Eastern Mediterranean Region. Geoogical Society of America Special Paper, vol. 409, pp. 237–258.

Marchev, P., Georgiev, S., Zajacz, Z., Tommasini, S., Manetti, P., von Quadt, A., 2007. High-K ankaramitic and high-Al magmas in the Eastern Srednogorie continental arc: comparison between melt inclusion geochemistry and lavas. Advances in Regional Geological and Metallogenic Studies in the Carpathians, Balkans, Rhodope Massif and Caucasus (Romania, Serbia, Bulgaria and Georgia). Bor, Serbia.

Médard, E., Schmidt, M.W., Schiano, P., 2004. Liquidus surfaces of ultra-calcic primitive melts: formation conditions and sources. Contributions to Mineralogy and Petrology 148, 201–215.

Médard, E., Schmidt, M.W., Schiano, P., Ottolini, L., 2006. Melting of amphibole-bearing wherlites: an experimental study on the origin of ultra-calcic nepheline-normative melts. Journal of Petrology 47, 481–504.

Metrich, N., Clocchiati, R., 1996. Sulfur abundance and its speciation in oxidized alkaline melts. Geochimica et Cosmochimica Acta 60, 4151–4160.

Mehnert, K.R., 1975. The Ivrea zone. A model of the deep crust. Neues Jahrbuch für Mineralogie. Abhandlungen 125, 156–199.

Miller, D.J., Christensen, N.I., 1994. Seismic signature and geochemistry of an island arc: a multidisciplinary study of the Kohistan accreted terrane, northern Pakistan. Journal of Geophysical Research 99, 11623–11642.

Patrascu, S., Bleahu, M., Panaiotu, C., Panaiotu, C.E., 1992. The Paleomagnetism of the Upper Cretaceous magmatic rocks in the Banat area of South Carpathians — tectonic implications. Tectonophysics 213, 341–352.

Patrascu, S., Panaiotu, C., Seclaman, M., Panaiotu, C.E., 1994. Timing of rotational motion of Apuseni Mountains (Romania) — paleomagnetic data from Tertiary magmatic rocks. Tectonophysics 233, 163–176.
Petrelli, M., Poli, G., Perugini, D., Peccerillo, A., 2005. PetroGraph: a new software to visualize, model, and present geochemical data in igneous petrology. Geochemistry Geophysics Geosystems 6, Q07011. doi:10.1029/2005GC000932.
Popov, P., 1981. Magmotectonic features of the Banat-Srednogorie Belt. Geologica Balcanica 11, 43–72.
Popov, P., 1987. Tectonics of the Banat Srednogorie Rift. Tectonophysics 143, 209–216.
Popov, P., Kovachev, V., Strashimirov, S., Zhelev, V., Arnaudova, R., Banushev, B., Stavrev, P., Radichev, R., 1993. Geology and metallogeny of the Burgas Ore Region. University of mining and geology "St. Ivan Rilski". 93 pp.
Popov, P., Berza, T., Grubic, A., Ioane, D., 2002. Late Cretaceous Apuseni–Banat–Timok–Srednogorie(ABTS) magmatic and metallogenic belt in the Carpathian–Balkan orogen. Geologica Balcanica 32, 145–162.
Putirka, K., 1997. Magma transport at Hawaii: inferences based on igneous thermobarometry. Geology 25, 69–72.
Putirka, K., Johnson, M., Kinzler, R., Longhi, R., Walker, D., 1996. Thermobarometry of mafic igneous rocks based on clinopyroxene–liquid equilibria, 0–30 kbar. Contributions to Mineralogy and Petrology 123, 92–108.
Putirka, K.D., Mikaelian, H., Ryerson, F., Shaw, H., 2003. New clinopyroxene–liquid thermobarometers for mafic, evolved, and volatile-bearing lava composition, with applications to lavas from Tibet and the Snake River plain, Idaho. American Mineralogist 88, 1542–1554.
Putirka, K.D., Perfit, M., Ryerson, F.J., Jackson, M.G., 2007. Ambient and excess mantle temperatures, olivine thermometry, and active vs. passive upwelling. Chemical Geology 241, 177–206.
Quick, J.E., Singoi, S., Mayer, A., 1994. Emplacement dynamics of a large mafic intrusion in the lower crust, Ivrea-Verbano zone, northern Italy. Journal of Geophysical Research 99, 21559–21573.
Rickwood, P.C., 1989. Boundary lines within petrologic diagrams which use oxides of major and minor elements. Lithos 22, 247–263.
Ringuette, L., Martignole, J., Windley, B.F., 1999. Magmatic crystallization, isobaric cooling, and decompression of the garnet-bearing assemblages of the Jijal sequence (Kohistan terrane, western Himalayas). Geology 27, 139–142.
Rivalenti, G., Rossi, A., Siena, F., Singoi, S., 1984. The layered series of the Ivrea–Verbano igneous complex, Western Alps. Italy. Tschermaks Mineralogische und Petrographische Mitteilungen 33, 77–99.
Schiano, P., Eiler, J.M., Hutcheon, I.D., Stolper, E.M., 2000. Primitive CaO-rich, silica-undersaturated melts in island arcs:evidence for the involvement of clinopyroxene-rich lithologies in the petrogenesis of arc magmas. Geochemistry, Geophysics, Geosystems 1 (1999G000032).
Schmidt, M.W., Green, D.H., Hibberson, W.O., 2004. Ultra-calcic magmas generated from Ca-depleted mantle: an experimental study on the origin of ankaramites. Journal of Petrology 45, 531–554.
Sigurdsson, I.A., Kamenetsky, V.S., Crawford, A.J., Eggins, S.M., Zlobin, S.K., 1993. Primitive island arc and oceanic lavas from the Hunter ridge-Hunter fracture zone. Evidence from glass, olivine and spinel compositions. Mineralogy and Petrology 47, 149–169.
Smith, D.R., Leeman, W.R., 2005. Chromian spinel–olivine phase chemistry and the origin of primitive basalts of the southern Washington Cascades. Journal of Volcanology and Geothermal Research 140, 49–66.
Spandler, C., O'Neil, N.S.t.C., Kamenetsky, V.S., 2007. Survival times of anomalous melt inclusions from element diffusion in olivine and chromite. Nature 447, 303–306.
Stampfli, G.M., Borel, G., 2004. The TRANSMED transect in space and time: constraints on the paleotectonic evolution of the Mediterranean domain. In: Cavazza, W., Roure, F., Spakman, W., Stampfli, G.M., Ziegler, P. (Eds.), The TRANSMED Atlas: the Mediterranean Region from Crust to Mantle. Springer Verlag, Berlin, pp. 53–90.
Stanisheva, G., 1965. Ultrabasic volcanites in the Tamarin bakadjik, district of Yambol. Review of the Bulgarian Geological Society 26 (2), 135–156 (in Bulgarian with English abstract).
Stanisheva, G., 1968. New data on the volcanism of the Eastern Srednogorie. Jubilee Geological Volume 395–406 (in Bulgarian with French abstract).
Stanisheva, G., 1969. Leucite basanites in the Tamarino Bakadzhik, district of Jambol Yambol. Bulletin of the Geological Institute. Series Geochemistry, Mineralogy and Petrography 18, 233–253 (in Bulgarian with English abstract).
Stanisheva, G., 1970. Limburgites from the trachybasaltic formation in the Yambol District. Bulletin of the Geological Institute. Series Geochemistry, Mineralogy and Petrography 19, 189–199 (in Bulgarian with English abstract).
Stanisheva-Vassileva, G., 1980. The Upper Cretaceous Magmatism in Srednogorie Zone, Bulgaria: a classification attempt and some implications. Geologica Balcanica 10 (2), 15–36.
Stanisheva-Vassileva, G., 1989. East Srednogorie volcano-intrusive area. In: Stanisheva-Vassileva, G., Strashimirov, S., Yanev, Y. (Eds.), Alpine Magmatism and Related Metallogeny in Srednogorie and Eastern Rhodopes-XIV Congress Carpathian Balkan Geological Association, Sofia, Field Trip Guide Book. Sofia University, Sofia, pp. 27–38 (in Russian).
Stanisheva-Vassileva, G., Daieva, L., 1990. Across-arc geochemical variations of Late-Cretaceous magmatism in the Eastern Srednogorie, Bulgaria. Geologica Balcanica 20 (4), 78.
Sun, S.S., McDonough, W.F., 1989. Chemical and isotopic systematics of oceanic basalts: implications for mantle composition and processes. In: Saunders, A.D., Norry, M.J. (Eds.), Magmatism in the ocean basins, pp. 313–345.
Sun, C.-H., Stern, R.J., 2001. Genesis of Mariana shoshonites: contribution of the subduction component. Journal of Geophysical Research 106 (B1), 589–608.
Turner, S., Arnaud, N., Liu, J., Rogers, N., Hawkesworth, C., Harris, N., Kelly, S., van Calsteren, P., Deng, W., 1996. Post-collision, shoshonitic volcanism on the Tibetan Plateau: implications for convective thinning of the lithosphere and the source of ocean island basalts. Journal of Petrology 37, 45–71.
Ulmer, P., 1989. The dependence of the Fe^{2+}–Mg cation-partitioning between olivine and basaltic liquid on pressure, temperature and composition — an experimental-study to 30 Kbars. Contributions to Mineralogy and Petrology 101, 261–273.
Yosifov, D., Pchelarov, V., 1977. A scheme of the thickness of the Earth's crust in the Balkan Peninsula and some features of its structures. Geologica Balcanica 7, 7–22 (in Russian, with English abstract).
Zajacz, Z., Halter, W., 2007. LA-ICP-MS analyses of silicate melt inclusions in co-precipitated minerals: quantification, data analysis and mineral/melt partitioning. Geochimica et Cosmochimica Acta 71, 1021–1040.
Zajacz, Z., Kovács, I., Szabá, C., Halter, W., Pettke, T., 2007. Evolution of mafic alkaline melts crystallized in the uppermost lithospheric mantle: a melt inclusion study of olivine-clinopyroxenite xenoliths, Northern Hungary. Journal of Petrology 48, 853–883.